



The provenance of Danubian loess

Kaja Fenn^{a,b,*}, Ian L. Millar^c, Julie A. Durcan^b, David S.G. Thomas^b, Adriano Banak^d, Slobodan B. Marković^e, Daniel Veres^f, Thomas Stevens^g

^a Department of Geography and Planning, University of Liverpool, Liverpool L69 7ZT, UK

^b Oxford University Centre for the Environment, South Parks Road, Oxford OX1 3QY, UK

^c Geochronology and Tracers Facility, British Geological Survey, Keyworth, Nottingham NG12 5GG, UK

^d Croatian Geological Survey, Department of Geology, Sachsova 2, HR-10000 Zagreb, Croatia

^e Faculty of Sciences, University of Novi Sad, Trg Dositeja Obradovića 3, 21000 Novi Sad, Serbia

^f Romanian Academy, Institute of Speleology, Clinicilor 5, 400006 Cluj-Napoca, Romania

^g Department of Earth Sciences, Uppsala University, Villavägen 16, 752 36 Uppsala, Sweden

ARTICLE INFO

Keywords:

Geochronology

U-Pb

Hf isotopes

Quaternary

Loess-palaeosol sequences

Aeolian

Zircon

Fluvial

ABSTRACT

With one of the largest watersheds in Europe, draining complex geological terrains within the Alps, Bohemian Massif, Carpathians, Dinarides, and the Balkan Mountains, the Danube River valley has long been linked to the formation of thick loess deposits, particularly within the Middle and Lower Danube basins. However, uncertainty over the provenance of loess-palaeosol sequences along the Danube impacts our understanding of sediment generation mechanisms and hinders interpretation of paleoenvironmental proxies preserved in loess. To date, most of the studies investigating loess provenance in Europe have not attempted a standardised characterisation and synthesis of loess deposits with potential source rocks. Further, despite clear links identified between loess and rivers in Asia and Europe, detrital zircons have not yet been used systematically to investigate the relationship between loess and the fluvial sediments of the Danube and its tributaries. Finally, in European loess research, provenance fingerprinting has often been conducted using indirect approaches or bulk sample geochemical analyses, which have been shown to have a limited application in well mixed sedimentary bodies such as loess.

This provenance study of loess along the Danube River integrates existing zircon U-Pb ages and Hf datasets for loess, rivers, and bedrock, with new loess zircon U-Pb and Hf results from loess sequences in Croatia, Serbia and Bulgaria. The results show that all surrounding mountain belts (i.e. the Alps, Bohemian Massif, Carpathians, Dinarides Alps, and Balkan Mountains) contribute primary sediment to loess deposits in the Danube valley via its modern tributary network. Critically sedimentary sources remain relatively homogenous along the river, with no apparent major change in source with tributary confluence, further highlighting the role of fluvial transport in homogenising sediment prior to final aeolian deposition. Whilst some small site variations can be observed, they are likely explained by contributions restricted to very local rock outcrops. Moreover, geomorphological results support floodplain sediments as the proximal sediment source and suggest that short-distance aeolian transport dominates sediment delivery to loess sequences, challenging distant sources hypotheses such as major Saharan sources. The identification of sediment sourced from lower elevation regions such as the Bohemian Massif, Dinarides, and Balkans, which did not support ice-caps, suggests that the role of glacial action in silt-size sediment production has been previously exaggerated. Therefore, the glacial and desert loess division inadequately separates and describes sediment generation processes. This research supports and furthers previous work, which suggests “mountain sourced and transported by-rivers” as a more appropriate term for the particles forming loess, at least in the Danube basin.

* Corresponding author at: Department of Geography and Planning, University of Liverpool, Liverpool L69 7ZT, UK.

E-mail address: kaja.fenn@liverpool.ac.uk (K. Fenn).

<https://doi.org/10.1016/j.earscirev.2022.103920>

Received 24 June 2021; Received in revised form 17 November 2021; Accepted 6 January 2022

Available online 15 January 2022

0012-8252/© 2022 The Authors. Published by Elsevier B.V. This is an open access article under the CC BY license (<http://creativecommons.org/licenses/by/4.0/>).

1. Introduction

Loess deposits along the Danube river have been accumulating since at least the mid-Quaternary (Jordanova et al., 2008; Marković et al., 2011) and preserve some of the longest terrestrial records of palaeoenvironmental and palaeoclimatic changes in Central and Southeastern Europe (Marković et al., 2015). The primary sources of the silt-sized particles forming the majority of the Danubian loess in previously ice-covered mountainous regions (Bugge et al., 2008; Jipa, 2014; Lehmkuhl et al., 2021; Schatz et al., 2015; Smalley and Leach, 1978; Újvári et al., 2008; Újvári and Klötzli, 2015) are still debated, which impacts our understanding of sediment generation mechanisms and its regional dispersal by fluvial systems and other processes (Matenco et al., 2013). Additionally a lack of consensus over the dynamics of the secondary, geomorphological sediment storage pools (temporary holding areas), e. g. deflation from river terraces, floodplains, periglacial environments, or glacially derived deposits (Badura et al., 2013; Mahaney and Andres, 1991; Muhs, 2013a; Smalley, 1966), further hinders efforts to reliably constrain the sediment transport mechanisms and pathways of mineral particles (mainly silt-sized) forming loess deposits. Together these suppositions limit the application of loess studies to atmospheric dust activity research and impede interpretation of certain loess environmental proxies such as grain-size.

While debate still persists in the literature, glacial grinding and cold-climate weathering processes are widely thought to be the primary processes generating the fine particles that form loess, especially in high latitudes and mountain environments (Bullard, 2013; Mahaney and Andres, 1991; Muhs, 2013b; Smalley, 1966). Consequently, glacial grinding under the Fennoscandian Ice-Sheet was seen as capable of generating large quantities of silt size sediment. As a result, the Scandinavian Mountains and Shield were proposed as an important source area of Danubian loess (Smalley and Leach, 1978), with sediment delivered by glacial meltwater into the Danube River catchment area via the Moravian depression. However, based on loess bulk sample geochemistry, Bugge et al. (2008) excluded contributions from Scandinavian proto-sources, at least for loess investigated in Serbia.

The Alps and Carpathians have also been suggested to be the primary source regions for Danube loess, based on conceptual models (Smalley et al., 2009; Smalley and Leach, 1978), bulk sample elemental composition of loess from Serbia (Bugge et al., 2008) and Hungary (Újvári et al., 2008), and loess bulk sample Sr-Nd isotopes and detrital zircon U-Pb ages (Újvári et al., 2012). Some researchers have since advocated for the importance of smaller, more proximal, mountainous regions as sediment producers, such as the Bohemian Massif (Újvári et al., 2013; Újvári and Klötzli, 2015), Transdanubian Central Range (Thamó-Bozsó et al., 2014), Slavonian Mountains (Banak et al., 2012), and Balkan Mountains (Jipa, 2014). While the Alps were covered by an ice-cap, which was able to generate large volumes of fine grained sediment, the extent to which the Carpathian and Balkan Mountains or Bohemian Massif supported features larger than unconnected glacier lobes during glacial periods is debated (Engel et al., 2017; Hughes and Woodward, 2017; Klapýta et al., 2021; Mentlik et al., 2013; Urdea et al., 2011), and by implication it is unclear whether they could have generated the large quantities of silt size sediment sufficient to form the extensive Danube loess deposits. If areas without large ice sheets are also confirmed as source regions for the Danube loess deposits, then the postulated need for extensive glacial activity in silt production and ultimately loess formation may have been previously exaggerated.

Alluvium has often been emphasised as a major immediate, geomorphological source of loess deposits (Lehmkuhl et al., 2016, 2021; Smalley et al., 2009). The Danube's floodplains have been identified as loess sources by numerous researchers (Jipa, 2014; Pötter et al., 2021; Thamó-Bozsó et al., 2014; Újvári et al., 2014; Varga et al., 2013) implying they temporarily store sediment derived from the Alpine or Carpathian regions. These source signatures were noted in Danubian alluvium in Serbia (Bugge et al., 2008) and Hungary (Újvári et al.,

2008), which was subsequently considered as a proximal loess source at both localities. Other larger tributaries (e.g. Tisza, Drava, Sava, Olt, or Jiu) are seen as delivery routes for sediment from additional smaller source regions (Bösken et al., 2019; Jipa, 2014; Pötter et al., 2021; Schatz et al., 2015), however their isotopic source signatures have not been compared with the Danubian loess deposits and therefore little is known about their contributions.

Lastly, distal sediment holding areas, such as the Sahara Desert, have also been suggested based on analysis of particle size and modern dust sources (Stuut et al., 2009; Varga et al., 2013), past contributions to palaeosols (Varga et al., 2016), and dust flux and elemental composition in Carpathian peat bogs (Longman et al., 2017). The increased frequency and magnitude of dust storms originating from Africa during the glacial period are thought to be the mechanism behind any additional sediment delivery from the Sahara (Goudie and Middleton, 2001). However, so far Saharan geochemical signatures cannot definitively be confirmed in Danubian loess deposits due to the absence of indicator minerals (Újvári et al., 2012).

Potential variation of loess source material across the Pannonian Basin has only been briefly touched on in previous research, despite its relevance to understanding dust and sediment transport pathways. In a theoretical analysis, Smalley and Leach (1978) argued shifts in loess source likely occurred where new tributaries entered the Danube's system, e.g. the Moravian gate or Tisza confluence. Similarly Nemecz et al. (2000) compared the dolomite to calcite ratio in Hungarian and Serbian loess and argued that one of the tributaries (the Drava or Tisza) delivers more calcite to loess in Serbia, diluting the dolomite to calcite ratio, or that loess in Hungary receives larger inputs of dolomite than loess in Serbia (Kostić and Protić, 2000). In Croatian loess the potential importance of tributaries in shifting the loess provenance signal was demonstrated, where proximity to the Sava's alluvium and regionally exposed bedrock likely caused slight shifts in loess mineral assemblages (Banak et al., 2013). Bugge et al. (2008) compared bulk sample elemental composition between loess in the Dobrogea (Romania) and Pannonian Basin (Serbia) and argued for source variability, attributing the differences in the Dobrogea loess to inputs from other large glacio-fluvial sources in Ukraine. This result was further corroborated by Jipa's (2014) Lower Danube sediment transport model, which indicated that despite similarities, source variation between sites in Bulgaria and Romania could be observed and attributed to inputs from different tributaries and therefore laterally changing geologies. Recent bulk sample XRF analysis of the Lower Danubian loess by Pötter et al. (2021) showed that while local contributions can be discerned in loess records further from the Danube, the majority of the loess geochemical signal follows a consistent pattern corresponding to the Danube alluvium.

Consequently, source homogeneity across a region as large as the entire Danube Basin would suggest that either there is one dominant sediment source contributing to the region and suppressing other signatures, or large scale sediment mixing is taking place, which provides an "averaged" homogenous provenance signal in all deposits. Újvári et al. (2008) supported this latter idea, showing bulk sample geochemical uniformity between numerous loess-palaeosol profiles across south-western Hungary. Schatz et al. (2015) also argued for sediment homogeneity of loess in Tokaj, Hungary (Pannonian Basin) and Grub, Austria (Vienna Basin) based on bulk sediment elemental and isotopic composition. However, as the former is located in the foothills of the North Hungarian Mountains (West Carpathians) and the latter in the foothills of the Alps, it is unlikely that these sites share primary sources, but rather that their respective source rocks have similar compositions, which bulk sample geochemistry is not able to separate. Additionally, the hypothesis of multiple sources implies there could be numerous end-members for each given site that either contribute equally or are found on a mixing line. Loess bulk sample geochemistry may therefore not be an appropriate methodological approach for identifying sources of sediments that are typically well mixed as discussed by, e.g. Stevens et al. (2010), based on the analysis of loess from the Chinese Loess

Plateau.

U-Pb isotope analysis of zircon represents a powerful and widely used technique to analyse multiple single grains and assign multiple sediment sources to sediments, overcoming many of the limitations of bulk geochemical analyses (Stevens et al., 2010). While extensively used in Chinese loess (Bird et al., 2015; Che and Li, 2013; Fenn et al., 2018; Licht et al., 2016; Nie et al., 2015; Stevens et al., 2010; Zhang et al., 2021), to date only a handful of zircon U-Pb loess provenance studies have been conducted in Europe (Baykal et al., 2021; Pańczyk et al., 2020) with two on Danube (Újvári et al., 2012; Újvári and Klötzli, 2015) and only one of them presenting results of zircon Hf isotope analysis. The majority of studies use bulk sample elemental composition (Buggle et al., 2008; Obrecht et al., 2015; Pötter et al., 2021; Újvári et al., 2008),

or indirect approaches (such as geomorphological and mineralogical mapping (Jipa, 2014), theoretical approaches (Smalley et al., 2009; Smalley and Leach, 1978), or particle size (Bokhorst et al., 2011)), and do not carry out comparisons with source rocks, or previous geochemical studies. Therefore, they do not consider the full implications for palaeoclimate and sediment production on a broader sedimentary basin scale. Critically, while Ducea et al. (2018) have examined Lower Danube detrital zircon signatures within river sediments, no detailed synthesis or analysis of river sediment provenance from the entire Danube and tributaries currently exists. The study of sediment provenance in major rivers in loess areas has been shown to be critical in resolving questions over sediment routing in the Chinese Loess Plateau (Nie et al., 2015; Stevens et al., 2013). To overcome these limitations and systematically

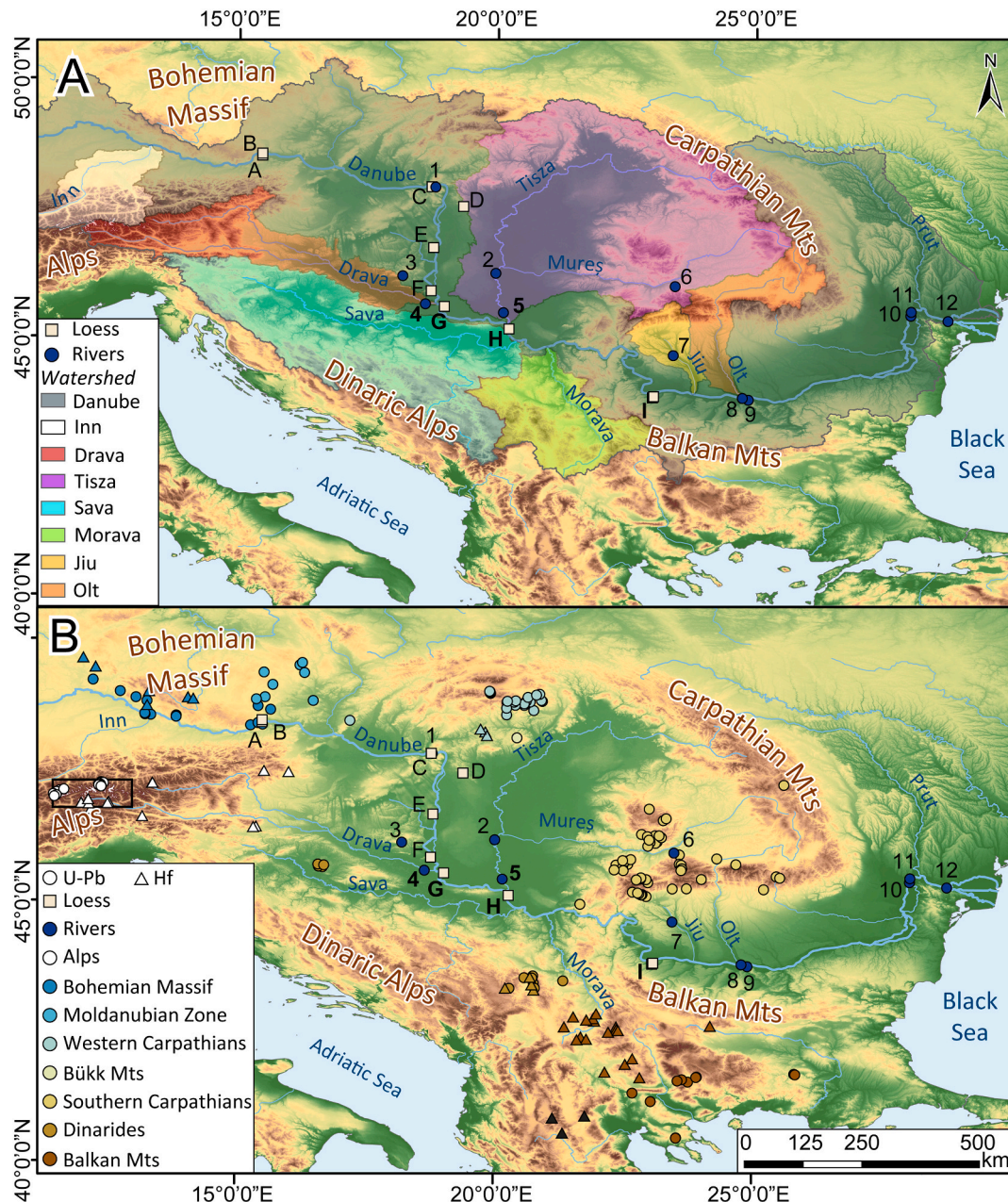


Fig. 1. A) Location of loess profiles, modern rivers, fluvial sediment and the catchments of the Danube and its main tributaries mentioned in the text. B) Location of primary source rocks, modern rivers, fluvial sediment and loess profiles mentioned in the text. Loess and fluvial sites analysed in this study are in bold. Capital letters refer to loess profiles A - Stratzing and Krems, B - Wels, C - Basaharc, D - Mende, E - Paks, F - Zmajevac, G - Erdut, H - Surduk 2, I - Slivata. Numbers refer to river sites: 1 - Basaharc fluvial sands, 2 - Tisza, 3 - Danita puszta fluvial sands, 4 - Drava, 5 - Tisza, 6 - Sebeşel, 7 - Jiu, 8 - Olt, 9 - Turnu, 10 - Tulcea, 11 - Siret, 12 - Braila. The black square marks the location of the Tauern Window. For source metadata see Supplementary Table S1 and S2. (DEM Source: ©JAXA).

investigate the provenance of Danube River and associated loess sediments, this study presents new detrital zircon U-Pb (3453 grains) results from 31 loess, palaeosol, and fluvial samples complemented by 210 existing loess, fluvial, and potential primary source rock datasets to constrain the source regions for loess material along the Danube River (Fig. 1) and explore spatial variability between sites. To overcome potential homogeneity of detrital zircon U-Pb ages between source regions, in addition to U-Pb dating, analysis of zircon Hf isotopes (3089 grains) is also conducted. The results of Hf isotope analysis are further compared to 57 published loess and primary source rock datasets.

2. Geologic setting

Central and Eastern Europe (Fig. 2) has a very complex geological history and is broadly composed of twelve tectonic units (Schmid et al., 2008). The region was shaped by several continental collisions, rifting, and mountain building events, which culminated with the collision of Africa and Eurasia, the closure of the Tethys Ocean, and associated Alpine Orogeny (2.5– 65 Ma). This final event is responsible for the uplift of the Alps, Carpathians, Dinaric Alps and Balkan Mountains that now surround the Pannonian Basin (Schmid et al., 2008, 2020; van Hinsbergen et al., 2020). Whilst this tectonic activity caused the present-day continental geography, many of the terranes were subject to multiple cycles of continental and oceanic pre-Alpine crustal and sedimentary reworking (Abbo et al., 2018; Avigad et al., 2017; Kroner and Romer, 2013; Meert, 2012; Meinhold et al., 2010, 2013; Spencer et al., 2013; Stampfli and Borel, 2002).

Of particular importance is the tectonic evolution since the assembly of Gondwana (750 Ma), since many crustal segments have been incorporated and now outcrop throughout Central Europe. The initial island arc formation throughout the Cryogenian and into the early Ediacaran (~ 720 – 600 Ma) resulted from the breakup of Rodinia and

development of the Mozambique Ocean, with continental collision forming the East African Orogen (Johnson et al., 2011; Stern, 1994). The final consolidation of the Gondwana supercontinent occurred between 650 and 550 Ma, and is associated with spatially varied Pan-African orogenic mountain building events, volcanism and magmatism (Cawood and Buchan, 2007; Hefferan et al., 2014; Küster and Harms, 1998; Meert, 2003; Nance et al., 2008; Squire et al., 2006; Veevers, 2003, 2007). During the late Neoproterozoic at Gondwana's northern active margins, a series of detached basement blocks (peri-Gondwana terranes) began to develop (von Raumer et al., 2003; Zeh and Gerdes, 2010), and were eventually separated from the supercontinent by the opening of the Rheic ocean ~485– 465 Ma (Nance et al., 2012; Stampfli et al., 2013; Stampfli and Borel, 2002; von Raumer et al., 2015). The widespread Pan-African uplift events translated into enhanced erosion and weathering, recycling and subsequent deposition of sediment on the peri-Gondwanian shelf by a complex fluvial and fan system (Abbo et al., 2018; Avigad et al., 2017; Hefferan et al., 2014; Iizuka et al., 2013; Meinhold et al., 2013; Wang et al., 2019).

At the western margins of Gondwana rifting events during the Cambrian and Early Ordovician (540 – 470 Ma), that led to the development of the Rheic Ocean, resulted in the detachment of Avalonia (Burda et al., 2021; Linnemann et al., 2012; Nance et al., 2012; von Raumer et al., 2003). The movement of Avalonia north-eastwards, progressively closing off the Tornquist Sea, culminated in the collision with Baltica by the late Ordovician and early Silurian, ~ 440 Ma (Oliver et al., 1993; Trench and Torsvik, 1992). The amalgamation of these two continental fragments resulted in the development of the Trans-European Suture Zone (Torsvik and Rehnström, 2003; Walczak and Belka, 2017), which was further reactivated during the Variscan and Alpine orogenies.

Further rifting from early Ordovician (~490 Ma) at the northern margin of Gondwana separated Cadomian terranes and led to the

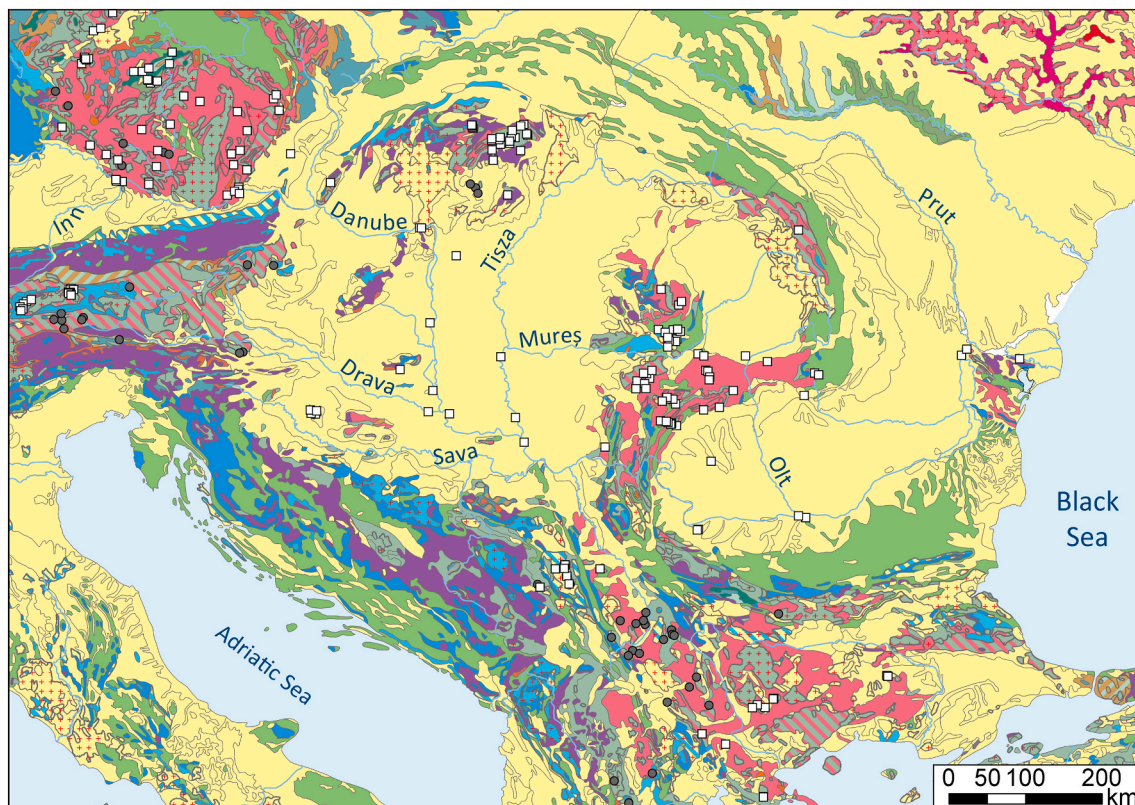


Fig. 2. Simplified geological map of the study region (adapted from Pawlewicz et al. (2002) and Persits et al. (1999)). White squares - location of U-Pb supporting datasets; black circles - location of the Hf isotope supporting datasets as outlined in Fig. 1. To aid clarity some periods have been combined based on the relevance to this research (e.g. Palaeogene, Neogene, and Quaternary).

development of Palaeo-Tethys (Stampfli et al., 2002; Stampfli and Borel, 2002; von Raumer et al., 2003, 2015). Both the Rheic and Palaeo-Tethys continued to operate, separated by Cadomia, until the closure of the Rheic Ocean ~ 280 Ma (Abbo et al., 2020; Nance et al., 2010) by the collision of Laurussia and Gondwana, which resulted in the Variscan Orogeny, and assembly of Pangea (Edel et al., 2018; Kroner and Romer, 2013; Stampfli et al., 2013; Stephan et al., 2019). The first phase of Pangea's break up began in the Triassic, however most reconstructions place the main stages of rifting in early to middle Jurassic, when the Tethys system began to open up (Rosenbaum and Lister, 2005; Schmid et al., 2008, 2020; Stampfli and Borel, 2002; van Hinsbergen et al., 2020). The gradual and complex events led to the separation of the Gondwana remnants, the closure of Tethys, concluding with the collision the African and European plates, the Alpine orogeny, and the modern-day distribution rocks seen in Fig. 2.

3. Methods

3.1. Sample collection and preparation

Approximately 2 kg of bulk sediment was collected from each sampling point at the Erdut (Croatia), Surduk 2 (Serbia), and Slivata (Bulgaria) loess-palaeosol profiles (Fig. 1). The stratigraphic position, lithology, and sample numbers are presented in Supplementary Table S3. The loess-palaeosol unit nomenclature is based on previous chronological studies at each site; Erdut (Fenn et al., 2020a), Surduk 2 (Fenn et al., 2020b), and Slivata (Fenn et al., 2021). The samples span two glacial-interglacial cycles, from the Holocene soil (S0) to the MIS 7 interglacial palaeosol (S2). Additionally, modern river sediment from the exposed sandy-silty alluvium was sampled from the Drava and Tisza Rivers (Fig. 1, points 4 and 5 respectively).

Loess is typically poorly sorted with a wide range of particle sizes, a larger proportion of clay in palaeosols and coarser silt and sands in loess units (Pye, 1995). The mean, median, and mode are all used to describe loess average grain size, which may lead to difficulties in grain size comparison. Nonetheless, typical loess in the Pannonian Basin has a mode in the range of 25–40 μm (Fenn et al., 2020a; Marković et al., 2006; Vandenberghe et al., 2014; Varga et al., 2019), a mean of 15–45 μm (Újvári et al., 2016; Varga et al., 2019), and a median of 15–40 μm (Újvári et al., 2016). Grain sizes below 20 μm are typically associated with palaeosols and do not contribute more than 20% to the particle size distribution (Antoine et al., 2009, 2019; Marković et al., 2008; Novothny et al., 2011). To achieve a balance between targeting the dominant fraction in loess sediment, ability to distinguish and avoid grains with complex internal structures or obvious metamorphic overgrowths, and isotope fractionation during the laser ablation ICP-MS, a 20 μm laser spot was used for U-Pb and a 25 μm spot for the Hf isotopes. Therefore all grains analysed were larger than 20 μm .

Sample preparation and analysis was carried out at the Geochronology and Tracers Facility of the British Geological Survey. First, 1 kg of sediment was subject to Stoke's settling to remove clay (<4 μm) from the bulk sediment. The remaining sediment was processed through a superpanner to concentrate heavy minerals and dried overnight in a drying cabinet. Next, heavy minerals were separated from the concentrate using heavy liquid (di-iodomethane; 3.3 g cm⁻³) and zircons enriched fractions extracted through magnetic separation by Frantz Isodynamic Separator. Zircon-enriched separates were mounted on epoxy disks (without picking, to avoid size and identification bias), and polished to reveal majority of grain centres. All grains were imaged using cathodoluminescence (Quanta FEI scanning electron microscope) prior to U-Pb and Hf analysis to create a stub map and help identify grains for measurement.

3.2. Detrital zircon U-Pb age analysis

To obtain U-Pb ages, imaged grains were analysed using two mass

spectrometer systems: a Nu Instruments AttoM single-collector inductively coupled plasma mass spectrometer (SC-ICP-MS); and a Nu Plasma HR multi-collector mass spectrometer (MC-ICP-MS). All samples were analysed using a 20 μm laser spot, with a 20 s laser warmup/sample washout, and a 30 s laser ablation dwell time (full analysis parameters can be found in Supplementary Table S4). Between two and four measurements of each of the reference materials (Plešovice zircon (Sláma et al., 2008), 91,500 (Wiedenbeck et al., 1995), and GJ-1 (Horstwood et al., 2016)) were conducted every ~30 grains to correct the instrument mass bias and depth dependent inter-element fractionation of U, Pb, and Th. All data were processed using a combination of Iolite data reduction software (Paton et al., 2011) and IsoplotR (Vermeesch, 2018a). For grains < 1.2 Ga, the ²⁰⁶Pb/²³⁸U age was used, whereas for older grains, the ²⁰⁷Pb/²⁰⁶Pb age was chosen. Ages were rejected if the discordance exceeded $\pm 10\%$. All raw data for samples and standards including element concentrations, ratios, and ages can be found in Supplementary Table S5.

3.3. Detrital zircon Hf isotope analysis

Following the U-Pb age analysis each grain was re-analysed for the Lu-Hf isotopic composition, targeting the same spot used for the U-Pb analysis. Isotope analyses were carried out at the British Geological Survey using a Thermo Scientific Neptune Plus MC-ICP-MS coupled to a New Wave Research UP193UC Excimer laser ablation system. Helium was used as the carrier gas through the ablation cell with Ar make-up gas being connected via a T-piece and sourced from a Cetac Aridus II desolvating nebulizer. 0.01 l/min of nitrogen were introduced via the nebulizer in addition to Ar in order to minimise oxide formation. Lutetium (¹⁷⁵Lu), Ytterbium (¹⁷²Yb, ¹⁷³Yb), and Hafnium (¹⁷⁶Hf, ¹⁷⁸Hf, ¹⁷⁹Hf and ¹⁸⁰Hf) isotopes were measured simultaneously during static 30 s ablation analyses. The spot size used was 25 μm ; fluence = 8 J cm⁻².

Hf reference solution JMC475 was analysed during the analytical session and sample ¹⁷⁶Hf/¹⁷⁷Hf ratios are reported relative to a value of 0.282160 for this standard. Reported ratios are relative to ¹⁷⁹Hf/¹⁷⁷Hf = 0.7325. Correction for ¹⁷⁶Yb on the ¹⁷⁶Hf peak was made using reverse-mass-bias correction of the ¹⁷⁶Yb/¹⁷³Yb ratio empirically derived using Hf mass bias corrected Yb-doped JMC475 solutions (Nowell and Parrish, 2001). ¹⁷⁶Lu interference on the ¹⁷⁶Hf peak was corrected by using the measured ¹⁷⁵Lu and assuming ¹⁷⁶Lu/¹⁷⁵Lu = 0.02653. Three zircon reference materials (91,500 (Blichert-Toft, 2008), Mud Tank (Woodhead and Hergt, 2005), and GJ1) were analysed throughout the analytical session at regular intervals (typically after every 40–50 unknowns). The 91,500 zircon reference material was used as the primary standard in Iolite, and was used to normalise the ¹⁷⁶Lu/¹⁷⁷Hf ratio assuming a value of 0.000311 (Woodhead and Hergt, 2005). Weighted mean ¹⁷⁶Hf/¹⁷⁷Hf values for the analysed standards are as follows: 91500, 0.282307 \pm 0.000003 (2 s), MSWD = 0.87, n = 304; GJ-1, 0.282017 \pm 0.000003, MSWD = 0.74, n = 286; Mud Tank, 0.282509 \pm 0.000003, MSWD = 0.82, n = 285. See Supplementary Table S6 for more detail.

Analytical uncertainties for unknowns were propagated by quadratic addition to include the standard error of the mean of the analysis and the reproducibility of the 91,500 reference material. ϵHf values were calculated using a ¹⁷⁶Lu decay constant of $1.867 \times 10^{-11} \text{y}^{-1}$ (Söderlund et al., 2004), the present-day chondritic ¹⁷⁶Lu/¹⁷⁷Hf value of 0.0336, and a ¹⁷⁶Hf/¹⁷⁷Hf ratio of 0.282785 (Bouvier et al., 2008). Hf-isotope data was processed using the Iolite data reduction package (Paton et al., 2011). All raw data for samples and standards including element concentrations, ratios, and ages can be found in Supplementary Table S7.

Hafnium isotope compositions are presented as ϵHf values, and represent the time-integrated deviation of a zircon's hafnium isotope composition in parts per 10,000 from the Chondritic Uniform Reservoir (CHUR) at the time of crystallisation (as determined by the measured U-Pb age).

3.4. Supporting datasets

To investigate the primary sources of the material for loess deposits, 160 U-Pb and 60 Hf isotope datasets for zircon were collected from published literature, which amounts to 10,507 and 648 grains respectively. The collected datasets comprise a range of sources including various sedimentary settings (loess, fluvial, alluvial, desert) and bedrock. Most of the datasets are located within the modern drainage of the Danube River (Fig. 1), however some of the potential source regions either lack data for comparison or data are very sparse. This is particularly evident for the Eastern Carpathians, and the full extent of the Balkan Mountains and Dinaric Mountains. However, to overcome this challenge datasets from rocks of same age (Fig. 2) are included as a proxy for the rocks within modern Danube Basin. It also has to be considered that while these rocks are presently not within the Danube drainage basin, little is known about the extent of palaeodrainage. Further zircon recycling and temporary storage in sedimentary bodies over geological timescales could mean that a small fraction of grains from rocks presently not found within the Danube drainage basin could still contribute to loess deposits.

Collected zircon U-Pb and Hf datasets were all recalculated and scrutinised following the methodology applied to the newly collected datasets. Published data were discarded based on the U-Pb discordance (outside the applied $\pm 10\%$), a mismatch between the U-Pb and Hf data, and in cases where discordant U-Pb data was used in the ϵHf calculation.

3.5. Data analysis and visualisation

The resulting 31 new datasets (29 loess-palaeosol and 2 fluvial) comprise 3453 zircon U-Pb ages and 3089 zircon Hf isotopic compositions. Zircon U-Pb ages were visualised through Kernel Density Estimation (KDE; Vermeesch, 2012) using the *detzrcr* R package (Kristoffersen et al., 2016). The datasets were compared with published loess, river, and source rock datasets through the multi-dimensional scaling statistical approach (MDS; Vermeesch, 2013). Related to Principal Component Analysis, MDS, aims to statistically simplify datasets by reducing them into two-dimensional ‘maps’, where similar data points are plotted in clusters and dissimilar ones are mapped far apart. The distance between points approximates distance in a mathematical sense (Vermeesch, 2018a, 2018b) and is calculated using a Kolmogorov-Smirnov (KS) statistic (Vermeesch, 2013). The “non-metric” algorithm, which ranks rather than approximates dissimilarities, was used for all MDS configurations. The results are plotted on the dimensionless MDS plot and range from -1 to 1 . Zircon Hf isotope–time evolution was plotted using the *detzrcr* R package (Kristoffersen et al., 2016). The Hf isotopic age data were further re-calculated to create a “heat map”, using a version of Kernel Density Estimation analysis modified for R (Botev et al., 2010).

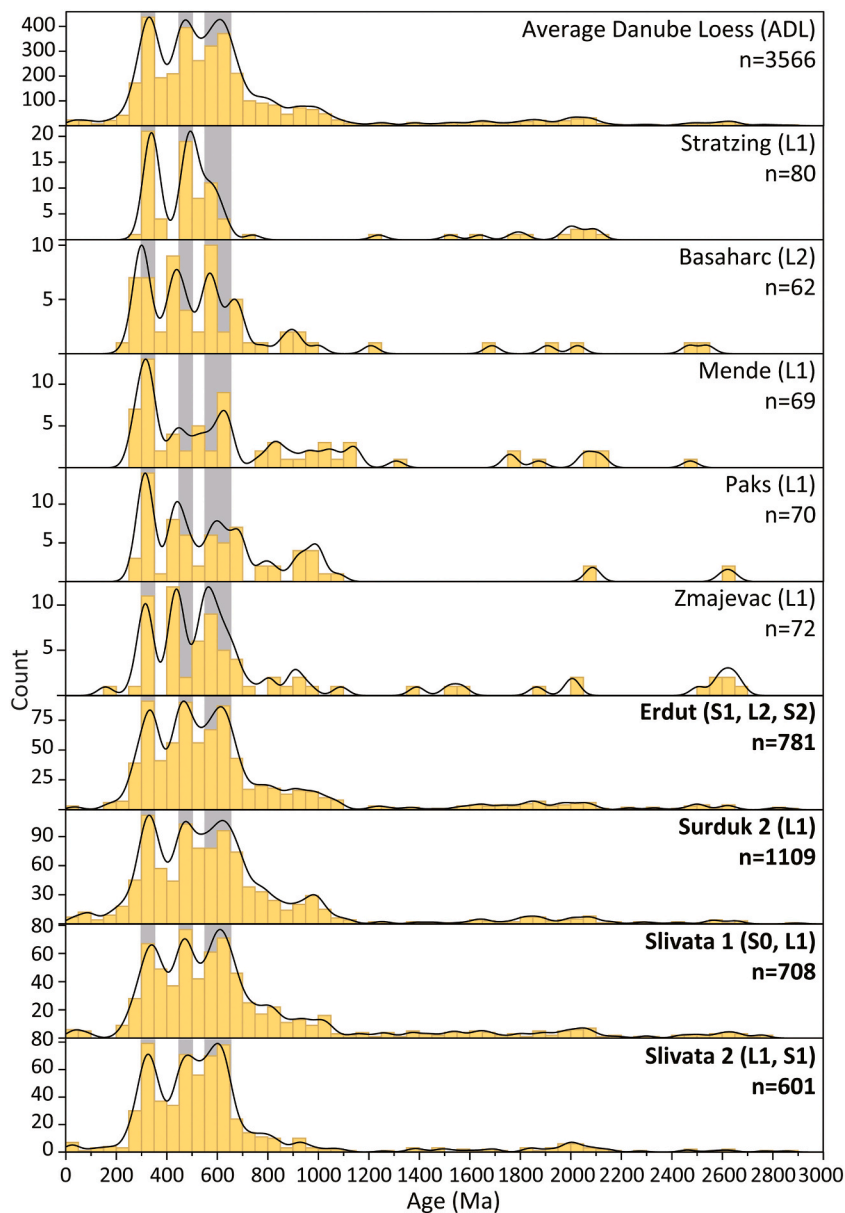
To focus on identifying the main primary sources of loess material in the Carpathian Basin and provide an overview of loess composition in the Danube catchment, the loess zircon U-Pb analysis from this work and previously published studies were combined to create an Average Danube Loess sample (ADL; 3566 data points). We note that this is an artificial sample and needs to be treated as such but by removing any potential inter-site variability this procedure provides a basis for investigating the overall characteristics of the main dataset and to fingerprint the dominant sources. In the second step focused on investigating geographical variability in source contributions along the Danube, U-Pb ages from loess and palaeosol units at each site were combined to create a site average. Importantly, the combined datasets for the sites investigated in this study (Erdut, Surduk 2, Slivata 1, and Slivata 2), are almost an order of magnitude larger than other loess datasets available in Europe. Therefore, in line with the suggestions of Vermeesch (2004) care must be taken when comparison is made to these relatively low grain number samples as populations $< 5\%$ might be absent due to the number of grains analysed.

4. Detrital zircon geochronology and Hf isotopic composition

The ADL’s KDE plot shows a continuous spread of zircon U-Pb ages (Figs. 3 and 4), with three dominant age populations of similar abundances at ~ 330 Ma (12.1%), ~ 450 Ma (11.1%), and 600 Ma (10.4%). These are more or less replicated in all loess samples from sites located near the Danube River, although the smaller proportion of grains in some of the populations at other sites are likely an artefact of smaller sample size. Grains with Carboniferous ages are common in all samples (11–20%) and in terms of a proto-source relate to the Variscan orogeny and associated magmatic events, as would be expected given the regional geology (Stephan et al., 2019). An alternative source for these grains could be (meta-) sedimentary rocks of Mesozoic-Cenozoic age, in which case they would represent zircon recycling. A Cambro-early Ordovician age peak appears in most samples, though in most cases it forms the smallest population (3–11%). These ages encompass a series of ocean floor spreading and closures, island arcs, and subduction zones that developed during collisions that produced proto-Europe (Kroner and Romer, 2013; Linnemann et al., 2014; Stampfli et al., 2013; von Raumer et al., 2003). Whilst samples from the loess profiles at Basaharc, Mende, Paks and Zmajevac contain a population of 400–450 Ma grains this population is younger and rather relates to late Ordovician-Silurian events. Finally, the ~ 600 Ma population associated with Gondwana-derived sources (Fielding et al., 2017; Zeh and Gerdes, 2010) consistently provides a large proportion of grains in all samples, though at the Paks and Zmajevac loess profiles the age peaks are centred around 550 Ma. All sites have a long Tonian tail (700–1000 Ma) and some smaller populations around 2000 Ma and 2500 Ma. Only 1.6% of zircon grains in the ADL are older than 2.5 Ga, and at individual sites this varies between 1% (Slivata 2) and 9.7% (Zmajevac), with Mende containing no such grains at all. A small change in the young grain age spectra is also observed, with <100 Ma almost absent at Erdut (0.3%), 1.9% at Surduk 2, 1.8% at Slivata 1, and 1.3% at Slivata 2 (Figs. 3, 4, and Supplementary Fig. S1). Crucially the relative proportion of grains represented by each peak shows only minor inter-site variability (Fig. 4).

Zircon U-Pb ages are combined with *in situ* obtained hafnium isotope data, where each grain’s age is plotted against its initial ϵHf value at the time of its crystallisation (Fig. 5). Depleted mantle rocks have $^{176}\text{Lu}/^{177}\text{Hf}$ values higher than CHUR, so develop positive ϵHf compositions through time. Crustal rocks in general have low $^{176}\text{Lu}/^{177}\text{Hf}$, so evolve negative ϵHf compositions. The depleted mantle (DM) evolution line in Fig. 5 is derived using present-day values of $^{176}\text{Hf}/^{177}\text{Hf} = 0.28325$ and $^{176}\text{Lu}/^{177}\text{Hf} = 0.0384$ (Griffin et al., 2006). Zircon grains with positive ϵHf values (between the CHUR and DM lines) are interpreted as sourced from juvenile magmas while negative values (below the CHUR) indicate zircons crystallised from re-melted crust. Granites formed in subduction-related, or collisional / post-collisional settings typically show a range in hafnium isotope compositions reflecting mixing between depleted mantle sources and melts derived from ancient crust. In the case of the Danubian loess detrital zircon hafnium compositions mostly fall between the depleted mantle evolution line, and the evolution trend of 3500 Ma crust. This range of compositions is similar to that shown by Gondwana-derived sedimentary sequences (e.g. Fielding et al., 2017). However, the great majority ($\sim 80\%$) of the zircons in the loess have only mildly negative ϵHf (0 to -10), indicative of remelting of relatively juvenile crust, or a relatively small contribution of non-radiogenic hafnium from more ancient crust. However contributions from Palaeoproterozoic or older crust are minor as within each major age population only a small proportion ($\sim 2.6\%$) of grains have ϵHf lower than -20 .

In detail, the Hf isotope–time evolution for the ADL (including only samples analysed in this study) (Fig. 5) shows three fairly well-defined peaks and three maxima in ϵHf –age space. Variations in the dominant age peaks are mostly attributed to differences in the proportions of juvenile and mature crust grains for the same age population. The highest concentration of grains is found for the 330 Ma population, though the



cluster is not well defined, with the majority of values found between 0 (upper quartiles) and -5 (lower quartiles). The 450 Ma peak is represented by very similar cluster of slightly negative ϵHf values (-0.35 to -5 , upper and lower quartile respectively), with a nominally more defined concentration in comparison to the 330 Ma population cluster. The 600 Ma population shows the widest discontinuity between density “hotspots” for the age grouping, with both juvenile ϵHf ($+3 <$) as well as crustal contributions (<-5), suggesting at least two different sources contributing to this age peak. Both 330 and 450 Ma populations may reflect zircon growth in magmas derived by melting of Neoproterozoic mafic crust. However to explain the strongly negative values shown by some data points at c. 600 Ma some involvement of melts derived from Palaeoproterozoic or older crust is required. These grains plot along the evolution line for the 3000–3500 Ma North African crust (Fielding et al., 2017). Lastly some variability can be observed in the young age spectra at ~ 50 and 100 Ma and a continuous ϵHf spread from $+5$ to -10 , indicating mixing between depleted mantle-derived and more mature crustal hafnium and potentially volcanic arc setting.

5. Discussion

U-Pb zircon datasets, for individual sites and for the ADL, were compared with 10,507 zircon grains from 160 published datasets from rivers, deserts, exposed outcrops, and mountain belts (Figs. 3 and 6), encompassing a variety of potential Central European source terranes. Bedrock and fluvial datasets were combined where possible (e.g. when reflecting the same geological units and ages) to reduce dataset complexity prior to MDS analysis (Fig. 7). Potential source area KDE plots (Fig. 6) show that to some degree most source samples contain the dominant populations represented in the ADL (grey area) and individual loess samples, demonstrating that any combination of these locations could be contributing to the loess deposits along the Danube, and emphasising the geological complexity of Central and Southeastern Europe. This is also reflected on the MDS map (Fig. 7) as most of the source datasets plot in one main group, comprising bedrock samples clustering around the loess and rivers, as discussed in section 5.2. The remaining bedrock samples from the Balkan, Dinarides, and Carpathian Mountains are spread to the side.

Fig. 3. Zircon U-Pb Kernel Density Estimator (KDE) diagram for the Average Danube Loess (ADL) sample and loess-palaeosol profiles (ordered from upstream to downstream) marked in Fig. 1 (A – Stratzing and Krems, B – Basaharc, C – Mende, D – Paks, E – Zmajevac, F – Erdut, G – Surduk 2, H – Slivata). 25 Ma bandwidth, 50 Ma binwidth, and Gaussian kernel were used for all diagrams. Grey shading marks the three dominant populations seen in ADL. Results from this study are marked in bold. For each loess site datasets from various units were combined. The chronostratigraphic position of each unit is indicated in brackets; S0 – Holocene soil, L1 – last glacial loess, S1 – last interglacial palaeosol, L2 – penultimate glacial loess, S2 – penultimate interglacial palaeosol. Dataset sources: Paks, Mende, Basaharc, Zmajevac (Újvári et al., 2012), and Stratzing combines Stratzing and Krems datasets (Újvári and Klötzli, 2015). See Supplementary Fig. S1 for the plot focused on 0–1000 Ma.

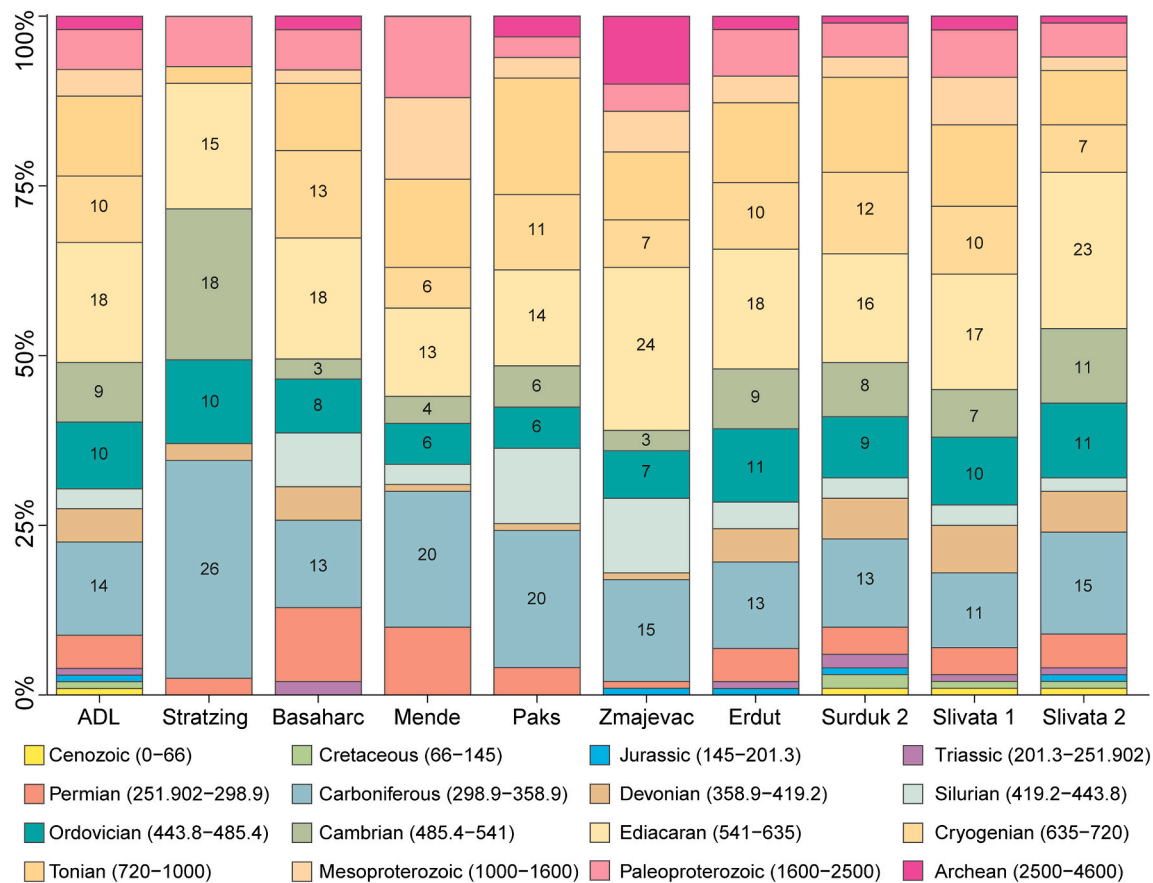


Fig. 4. Zircon U-Pb age proportions by geologic period (ages in Ma in parentheses) for samples shown in Fig. 3. Percentage values are given for periods that account for the three dominant populations in ADL (grey shading in Fig. 3).

5.1. Primary sources of Danube loess deposits

5.1.1. 600 Ma

The dominant c. 600 Ma age population corresponds to the Precambrian and Palaeozoic-Precambrian source rocks that can be found across Central and Southern Europe. These rocks represent fragments of peri-Gondwanan terranes that coalesced over several orogenic cycles and culminated in subduction-accommodating convergence since the Jurassic (Antić et al., 2016; van Hinsbergen et al., 2020; Zlatkin et al., 2018). These fragments may also preserve reworked Gondwana-derived sedimentary rocks with zircons of a distinctive Gondwanian age distribution (Meinhold et al., 2013). Moreover Gondwanian sources comprise Neoproterozoic arc terranes, syncollisional granites formed between 1000 and 600 Ma (Da Silva et al., 2005; Meira et al., 2015), and relicts of the Archaean and Palaeoproterozoic orogenies (Kouamelan et al., 2018; Meert, 2012). Zeh and Gerdes (2010) showed that Gondwana-derived sedimentary and igneous rocks can be found as far north as the Mid-German crystalline rise. A comparable pattern was reported in a detrital zircon study of the Nile catchment sources (NE Africa) by Fielding et al. (2017). Similarities in the tectonic origin and distribution of peri-Gondwanian terranes in Central and Southern Europe results in the abundance of a ~ 600 Ma population in source samples from most of the surrounding mountainous terrains (Fig. 6 and Fig. S1), which also translates to the large source rock cluster on the MDS (Fig. 7). Whilst a sample from the upper reaches of the Danube is unavailable, the presence of the 600 Ma populations in the Stratzing and Basaharc loess profiles (Újvári et al., 2012; Újvári and Klötzli, 2015) (Figs. 1 and 3) suggests that the Danube already carries grains of that age from its source. The 600 Ma population is further replenished by the River Inn (from the Alps) and smaller tributaries with headways in the Bohemian

Massif. These signatures are continuously replenished by the other tributaries (e.g. Drava and Tisza) along the way. The abundance of the 600 Ma grains in most source regions, and the large drainage area of the Danube River system which provides a constant supply of recycled Gondwanian material, means that these U-Pb ages cannot be used to distinguish source regions.

To investigate loess source further the Hf isotope time evolution for the ADL is plotted as a probability density plot with potential source data (Fig. 8). The Austroalpine Basement sample has two Neoproterozoic zircons age populations at ~ 600 Ma and 950 Ma that overlap well with the ADL dataset. Both distributions have a broad range of ϵ_{Hf} values at these ages extending to negative values indicative of zircons formed in melts of Archaean crust. A similarity in the Neoproterozoic ϵ_{Hf} isotope pattern can be seen in both the Drava River and the Austroalpine Basement samples (Figs. 8 and S3). As the Austroalpine Basement samples falls within the Drava drainage area (Fig. 1), the Drava River likely delivers these grains to the Danubian loess. Siegesmund et al. (2018) showed that these signatures are derived from Western Gondwana, which is in line with the typical Phanerozoic age of sediments in North Africa formed by erosion of the Pan-African orogen described by Fielding et al. (2017) and Fielding et al. (2018). Neoproterozoic outcrops of Gondwanian affinity are generally restricted in the Danube River basin, which is also supported by the lack of these ϵ_{Hf} isotopic values in the grains from the Tisza River (Figs. 8 and S3). Therefore the good match between the loess and the Austroalpine Basement south of the Tauern Window (black square in the Fig. 1B) supported by the Drava signatures, suggests the Austroalpine basement (or an as yet unidentified source with near-identical provenance) is a good candidate for a potentially large source of the 600 and 1000 Ma zircons for the Middle Danube's loess. Samples from the Dinarides and

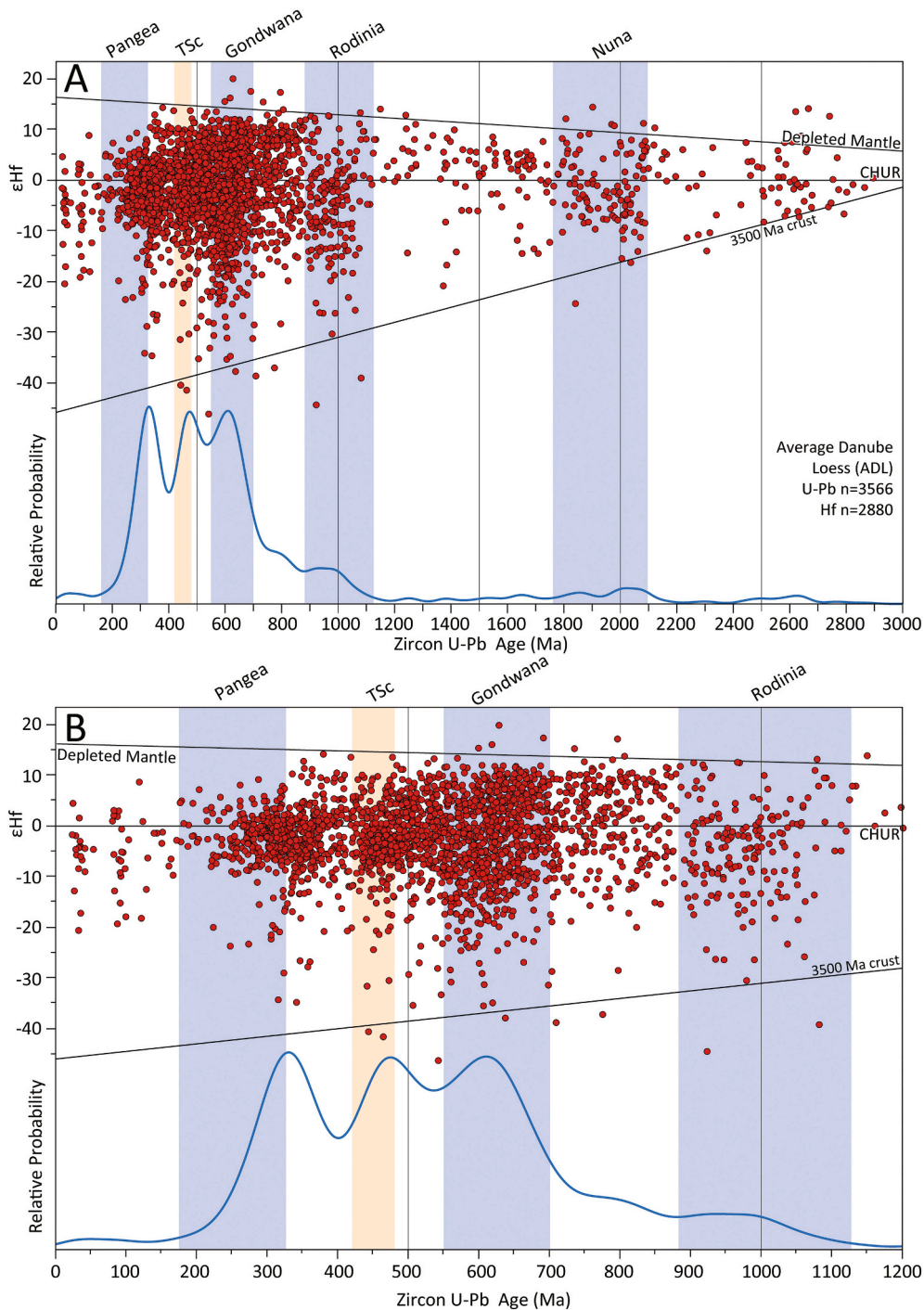


Fig. 5. Probability density plot showing Hf isotope-time evolution of Average Danube Loess (ADL) plotted together with U-Pb zircon ages. Panels: A) All datapoints; B) 0–1200 Ma interval. To illustrate the origins of zircon grains, the 3500 Ma crust evolution line and shading denoting supercontinent existence (blue shading) and Tornquist Sea closure (TSC; orange shading) are added. (For interpretation of the references to colour in this figure legend, the reader is referred to the web version of this article.)

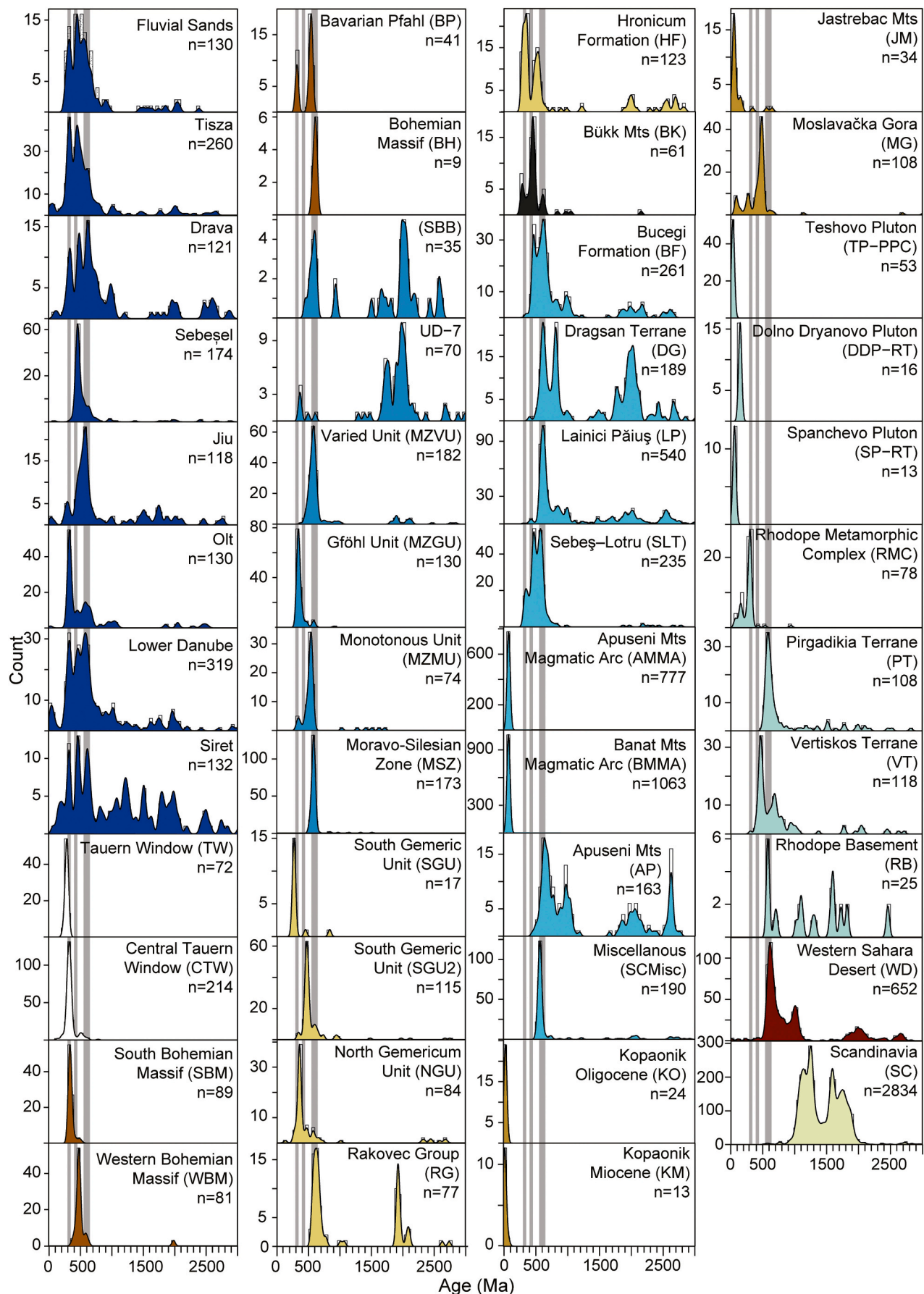
Hellenides (Vernon Massif) also have zircons with a positive ϵ_{Hf} (1.5–8), plotting as a decreasing trend from 500 to 800 Ma and together with 300 Ma samples from the Vorass Massif suggest an ~ 1370 Ma crust evolution line. However, while the 500–800 Ma Vernon Massif samples plot over the ADL distribution they do not contribute to the observed hotspots at 600 Ma (Figs. 5 and 8), but rather to smaller populations. Nonetheless this suggests that the Dinarides and Hellenides are also a plausible source of zircons to the Danubian loess.

5.1.2. 450 Ma

The second of the dominant ADL loess zircon populations is centred around ~ 450 Ma (Fig. 3), and the KDEs (Fig. 6) show that grains of these ages are also abundant in rocks across Central and Southern

Europe (Balintoni et al., 2014), e.g. the Bohemian Massif (WBM and SBM), Western Carpathians (SGU2), Bükk Mountains (BK), Southern Carpathians (BF and SLT), and Drava and Tisza rivers. The abundance of 450 Ma ages in Tisza sample and their presence in only some Southern and Western Carpathian samples could suggest that the Eastern Carpathians are one of the sources of the grains with these ages. However the limited number of source samples with ϵ_{Hf} isotope data (Fig. 8) available precludes investigation of the ADL's 450 Ma population source. There are hints of similarities with the Piemonte Zone, Schlading Complex, and especially the Serbo-Macedonian Massif, but no bedrock datasets explain the range of values seen, nor do they exactly overlap the 450 Ma ϵ_{Hf} “hot spot”.

In some loess profiles (Stratzing, Erdut, Surduk 2, and Slivata) this



(caption on next page)

Fig. 6. Zircon U-Pb Kernel Density Estimator (KDE) diagram for potential dust sources shown in Fig. 1 (colour coded): rivers (dark blue), the Alps (white), Bohemian Massif (brown), Moldanubian Zone (blue), West Carpathians (yellow), Bükk Mountains (black), South Carpathians (light blue), Dinaric Alps (ochre), Balkan Mountains (light turquoise), Sahara Desert (dark red), and Scandinavia (light green). Fluvial sands sample comprise Basaharc and Danitz pusztá fluvial sands (Fig. 1 points 2 and 5), Tisza includes two samples shown in Fig. 1 (2 and 5), and Lower Danube combines three datasets (Fig. 1 points 9, 10, 12). Grey shaded areas represent the three dominant populations seen in ADL. A 25 Ma bandwidth, 50 Ma binwidth, and Gaussian kernel were used for all diagrams. See Supplementary Table S1 for source metadata details and Supplementary Fig. S1 for higher resolution KDEs. (For interpretation of the references to colour in this figure legend, the reader is referred to the web version of this article.)

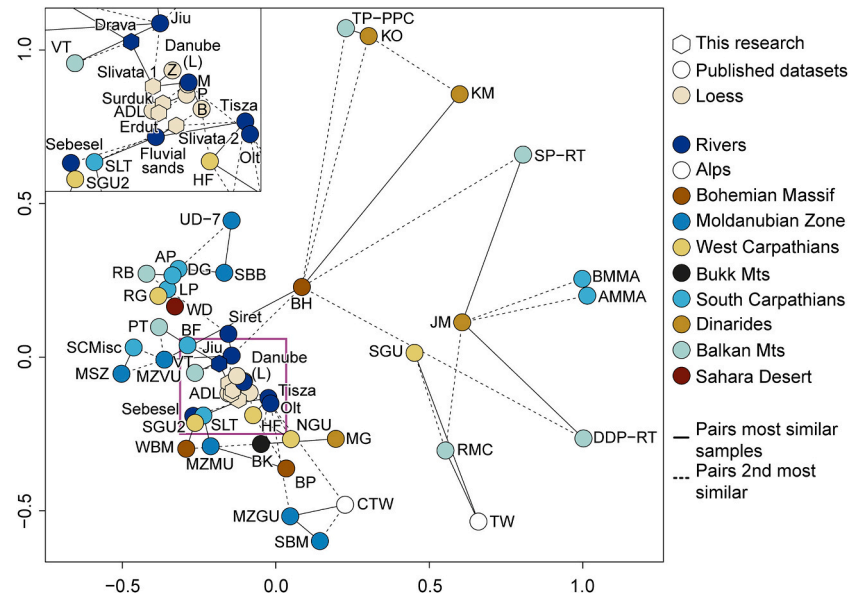


Fig. 7. Multi-dimensional scaling (MDS) diagram based on zircon data in Figs. 3 and 6, showing the average loess-palaeosol sample and potential dust sources. Insert - the enlarged loess data cluster (pink square). Abbreviations: B – Basaharc, M – Mende, P – Paks, Z – Zmajevac, Danube (L) – Lower Danube. See Supplementary Table S1 for source metadata. (For interpretation of the references to colour in this figure legend, the reader is referred to the web version of this article.)

peak is slightly older (~460–480 Ma) whereas at Basaharc, Mende, Paks and Zmajevac it sits ~430 Ma. This could be an artefact of smaller samples at the latter sites, or it could be linked to one of several events: two different phases of the events relating to the collision of the Avalonia and Cadomia terranes with the East European and North American Cratons and their multiple subduction zones (Kroner and Romer, 2013; Stampfli et al., 2013; von Raumer et al., 2003); Paleothetys opening (Haas et al., 2020); continental rifting related events (von Raumer et al., 2013); early Ordovician orogeny (Zurbruggen, 2015, 2017); or Tornquist Sea related subduction as a part of the Baltica and Avalonia collision (Oliver et al., 1993; Zurbruggen, 2015, 2017). Zircon Hf isotopes (Fig. 5) show a spread typically associated with volcanic arcs, with some relatively young magmas, a mixture of remelting of relatively juvenile crust, and mixing between depleted mantle sources and melts derived from ancient crust. The only overlap with the ADL's 450 Ma population (Fig. 8 and Supplementary Fig. S3) is provided by the Tisza sample, suggesting a source within Tisza's drainage. Additionally, the Tisza zircons show a decreasing trend between 450 and 330 Ma ages, from -3 to -5 respectively, which creates a crustal evolution line of ~1450–1500 Ma (Supplementary Figs. S3). Crust of that age has a non-Gondwanian affinity, and points to a Baltica origin (Bogdanova et al., 2006, 2008; Gee et al., 2014; Roberts et al., 2013). These grains could be linked to the final closure of the Tornquist Sea, and progressive spreading and subduction of the Rheic Ocean (Kroner and Romer, 2013; Nance et al., 2012; Oliver et al., 1993). At present these regions do not have a connection to the Danube's catchment, but these grains likely have been recycled and preserved within the drainage of Tisza.

Some similarities between ADL and the Balkan region are noted in both zircon U-Pb ages (Rhodopes Mountains; VT, RB, and PT) and Hf isotopes (Serbo-Macedonian Massif) in the 450 Ma range. At present these regions do not have a connection with modern Danube system and

neither of them can be a direct source of sediment for loess. However these source rocks can be taken as broadly representative of ages expected in the Balkan region, with some areas potentially providing small contributions via the Morava, Iskar, and other smaller tributaries. Moreover, some of the Balkan sources could have previously been connected to the Danube catchment as the present configuration is a relatively recent development (Matenco et al., 2013). Zircons could have been supplied to sedimentary rocks which are found within the Danube catchment at present, through cycles of erosion and deposition. Crucially Balkan region sources can only be considered as contributors to southern Serbian, Bulgarian, and Romanian loess. For the upper reaches of the Danube, the Bohemian Massif, West Carpathians, Bükk Mountains (Fig. 6), Black Forest Mountain's, where Danube has its headwaters (Chen et al., 2003; Fukum, 2002), and Alps (Haas et al., 2020; Huang et al., 2021; Loth et al., 2001; Schaltegger et al., 2003) are likely sources.

5.1.3. 330 Ma

The youngest (300–350 Ma) of the three loess zircon populations represents the Variscan orogenesis and Pangea building events that are preserved in rocks across Central Europe (Stephan et al., 2019). Fig. 6 shows these Carboniferous populations in the Alps (CTW and TW), Bohemian Massif (WBM, SBM, and BP), Moldanubian Zone (MZGU and MZMU), West Carpathians (SGU, NGU, HF), South Carpathians (SLT), Dinaric Alps (MG and JM) and Rhodope Mountains (RMC). These sources all plot relatively near the ADL and individual loess sites on the MDS diagram (Fig. 7), therefore any of these terrains could be a source for these grains. Hf isotopes (Fig. 5) show fairly typical subduction and/or collision related ranges of values, with some showing relatively negative ϵ_{Hf} , representing mixing between juvenile mantle sources and re-melted Paleoproterozoic-Archean crust. The highest concentration of

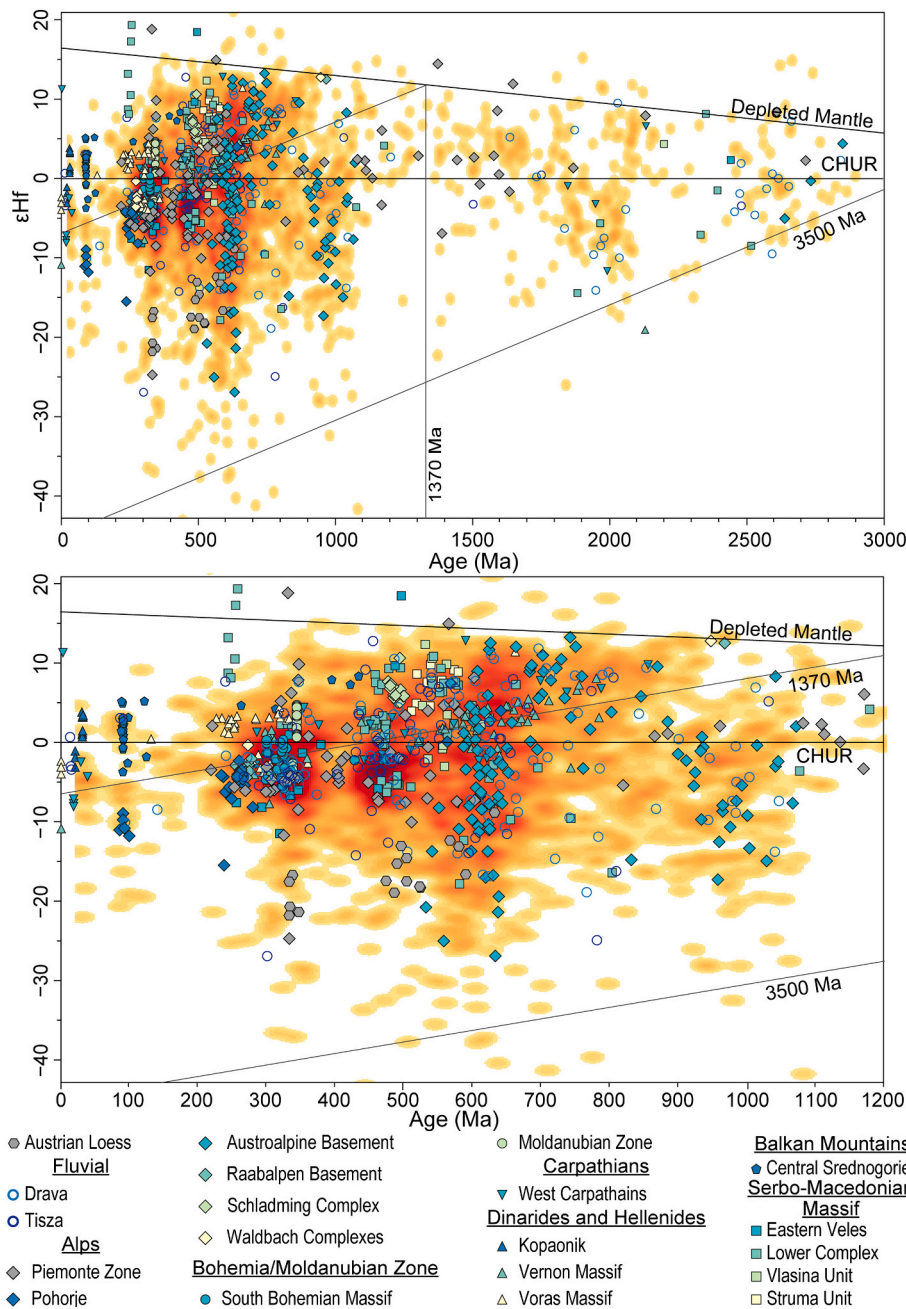


Fig. 8. Probability density plot showing Hf isotope-time evolution of the averaged Danubian loess, top panel shows all datapoints, whereas bottom panel shows 0–1200 Ma interval. The density of the data distribution is calculated using a modified version of the Kernel Density Estimation (Botev et al., 2010) analysis modified for R. ϵ Hf evolution lines for the 1370 Ma and 3500 Ma crust are added. The potential source Hf data are superimposed, see Supplementary Table S2 for the Hf metadata and Fig. S3 for overlap of individual potential sources.

source ϵ Hf data overlaps the ADL's 300 Ma population (Fig. 8), which is not surprising given the abundance of Mesozoic source rocks around the Pannonian Basin. Possible contributions come from various Alpine, Moldanubian, Bohemian, and Dinaric sources. A substantial overlap both with “the hotspot” and the range of values created by the South Bohemia Massif and Alps (e.g. Piemonte Zone) samples, implies that the regions draining directly into the upper reaches of the Danube (above the Inn confluence) are likely contributors of sediment for the ADL. Therefore, a significant quantity of sediment for loess deposits could be transported via the Danube before the river enters the Pannonian Basin. Additionally, the ADL's young zircon (<100 Ma) ϵ Hf clusters overlap with datasets from the Dinarides and Balkan Mountains. The analysis of U-Pb ages and Hf isotopes consistently points to the Dinaric and Balkan Mountains as sources of sediment for the loess deposits along the Lower Danube (past the Drava confluence), suggesting that these regions are much more important sediment sources than previously thought.

5.1.4. Scandinavia

To test for contributions from the Scandinavian sources a large “artificial” sample comprising Scandian nappes (Gee et al., 2014), Transscandinavian Igneous Belt (Lorentzen et al., 2018), and Southwest Scandinavian Domain (Roberts et al., 2013) was created (Fig. 6). This encompasses typical Scandinavian signatures that could be expected in the Danubian loess if the glacial outwash sediment was delivered via the Moravian Gate as proposed by (Smalley and Leach, 1978). The Scandinavian sample comprise three zircon age populations, two Mesoproterozoic (1000–1200 and 1450–1550 Ma) and Paleoproterozoic (1600–1700 Ma). Whilst a very minor Proterozoic tail is present in Danubian loess (Figs. 3 and 4) it is mostly comprised of Neoproterozoic grains and Mesoproterozoic signatures that are not very abundant and there is a general absence of the Paleoproterozoic ages. Therefore the comparison of the KDEs fairly robustly discounts Scandinavian sources and the glaciofluvial delivery route.

5.1.5. Primary sources

Zircon ages and hafnium isotopes show that several sources contribute to the Danube sediment and loess-palaeosol sequences in the Danube valley, i.e. there is no dominant source. However, it is not possible to discount the possibility of a more “dominant” source which is obscured by the similarity observed in the U-Pb age distributions between several sources. Further the fluvial mixing during sediment transport prior to the final aeolian deposition also complicates source identification. Thus, U-Pb zircon ages alone are unable to differentiate between source rocks in a complex geological setting and therefore multi-proxy approaches are necessary to resolve the source question. This multi-proxy analysis approach demonstrates that the ADL does not have a single lithological source, supporting findings of e.g. Jipa (2014), Schatz et al. (2015), Újvári et al. (2012), and Pötter et al. (2021). It also shows that to some extent all of the surrounding mountain belts (the Alps, Bohemian Massif, Carpathians, Dinarides, and Balkan Mountains) are primary sources of loess. However, the Hf isotope provides a strong additional tool that not only identifies new sources in the Dinaric and Balkan Mountains, but also identifies specific areas within mountain belts, i.e. Austroalpine Basement south of the Tauern Window in the Alps as large contributor of grains of 600–1000 Ma age especially to loess below Drava confluence.

5.2. Geomorphological source(s) of loess deposits

5.2.1. Fluvial link

River datasets are of particular interest as a catchment proxy, especially where published primary source zircon datasets from a potential source region might be largely missing e.g. Eastern Carpathians. This is particularly evident through the example of Siret River which mainly drains the Outer Carpathian Palaeozoic flysch system producing the similar three peak pattern but also has a large Proterozoic-Archean tail (absent in ADL) indicating old cratonic contributions likely from the Ukrainian shield.

The Lower Danube distribution (Fig. 6), representing the most averaged Danube signal having received sediment from its largest tributaries, has the most similar distribution to the ADL. Of the Danube's tributaries, the Drava and Tisza also have the three-peak distribution seen in the loess and Danube samples, despite draining different source regions (Alps for the Drava, and Carpathians for the Tisza). However, the dominance of these peaks is somewhat reversed, e.g. the 600 Ma population, dominant in the Drava by is by contrast relatively small in the Tisza, and the Tisza's dominant 300 Ma population is less abundant in the Drava. The dominance of the 300 Ma population as seen in the Tisza is also evident in the Olt River, with both rivers draining the Eastern and Southern Carpathians (Fig. 1A), suggesting an abundance of zircons of this age in this source region. However the geological variability of the region even over short distances, is also demonstrated by the dominance of Neoproterozoic grains in the Jiu River, which varies significantly from the Olt and drains a particularly old crustal segment of the Southern Carpathians (Dragan Terrane and Lainici Păiș; Fig. 6). Further, the insert in Fig. 7 shows that rivers with 300 and 600 Ma dominant distributions plot on opposite sides of the Danube samples. Two conclusions can be drawn from this. Firstly, some tributaries deliver the full spread of zircon ages to the ADL and loess samples, whilst others contribute only to a single but still dominant peak. Importantly they all likely contribute material to loess deposits. Second, sediment mixing from the surrounding sources occurs in the tributaries and the Danube, and the averaged signal is preserved in fluvial sediment, and in the alluvial plains.

The similar distributions between rivers and loess seen on the KDE plots (Figs. 3 and 6) also translate to proximity on the MDS plots (Fig. 7). The MDS plot shows that the ADL and all individual loess samples plot in the centre of the source cluster surrounded by river samples. Most source samples form a large cluster, which surrounds the river data but does not plot close to loess. This pattern suggests loess-forming sediment is first

eroded, transported, homogenised, and deposited by the rivers prior to the final aeolian transport and deposition, rather than transported directly from the primary sources with mixing in the air or via various multi-step processes. The mixed source terrane signals in the loess and Danube sediments (Figs. 3 and 6), supported by the different clustering between loess, rivers, and bedrock (Fig. 7), indicate that the proximal, geomorphological source of loess deposits along the Danube River is the Danube's alluvium, previously suggested as a source of silt to individual loess sites on the basis of theoretical, geomorphological, zircon U-Pb, and bulk sample geochemical investigations (Basarín et al., 2011; Bugle et al., 2008; Jipa, 2014; Pötter et al., 2021; Újvári et al., 2012).

Fig. 9 shows that loess deposits are typically located within 20 km (in most cases <10 km) of river channels and floodplains. Therefore by extension this suggests that at least during glacial periods short-distance aeolian transport dominates sediment delivery into loess deposits, whereas any long-distance transport contributions (> 1000's km) (Lehmkuhl et al., 2016; Obrecht et al., 2015; Rousseau et al., 2011; Varga et al., 2013, 2016) may be a feature predominant during warm phases. Further the relationship between river and bedrock datasets (Fig. 7) suggests that sediment mixing occurs during fluvial transport (and cycles of redeposition and erosion) rather than in the air during aeolian transport. Consequently this demonstrates that aeolian processes play only a secondary role in Danube basin loess genesis; the primary function is played by fluvial processes as previously suggested by Smalley et al. (2009), Újvári et al. (2013), and Újvári and Klötzli (2015). The importance of a fluvial link was also established by the provenance researches on the Chinese Loess Plateau, where Yellow River was ascertained to play a key role in sediment delivery prior to the aeolian redistribution (Bird et al., 2020; Licht et al., 2016; Nie et al., 2015; Stevens et al., 2013). Therefore whilst discussion over silt production mechanisms and loess transport modes persists in the literature, there is growing evidence, including this study, that supports the integral role river transport plays in the loess source-to-sink models generally (e.g. Lehmkuhl et al., 2016; Li et al., 2020).

5.2.2. Sahara Desert

A note on the long debated Saharan Desert source (Stuut et al., 2009; Újvári et al., 2012; Varga et al., 2016). The sample from the Western Desert, Egypt (WD) is located within the main data cluster on the MDS map (Fig. 7) and the detrital zircon U-Pb age distributions signatures (Fig. 6) highlight its 600 Ma Gondwanian signatures, suggesting possible Saharan contributions to grains in that age range. However, a large Saharan contribution would require mixing with material from other sources to produce the three peak distribution observed, as the Saharan sample does not contain the 330 and 450 Ma populations seen in the loess. Given that samples within the mountain belts surrounding the Danube basin also contain 600 Ma populations, as well as the Palaeozoic ones (Fig. 6), mixing of Saharan dust with local material would be required to yield all three populations in the loess. Indeed, if this was the case, a dominant 600 Ma peak could be expected at all sites, which is not seen in the data, suggesting that the 600 Ma grain contribution is more easily explained via Danube River sediment sources. Furthermore, factors beyond just the zircon U-Pb ages also need to be considered, including the impact of grain size and particle density on long-range aeolian transport capacity. Particle size (and the proportion of coarser grains) generally decreases with the distance away from source(s) under aeolian transport (Bagnold, 1941; Derbyshire et al., 1998; Lawrence and Neff, 2009; Mahowald et al., 2014). A shift in modal grain size away from coast of Sahara has been reported in several studies (Guerzoni et al., 1997; Skonieczny et al., 2013; Van Der Does et al., 2016), with Friese et al. (2017) showing over 66% reduction in mode within 500 km. Further modern studies of Saharan dust transport suggest that deposition of 60–90% grains above 30 μm occurs within 12 h of entrainment (Ryder et al., 2013). Whilst some have reported long-distance transport (3500 km) of particles above 100 μm (Middleton et al., 2001; Van Der Does et al., 2018; Varga et al., 2021), these represent modern,

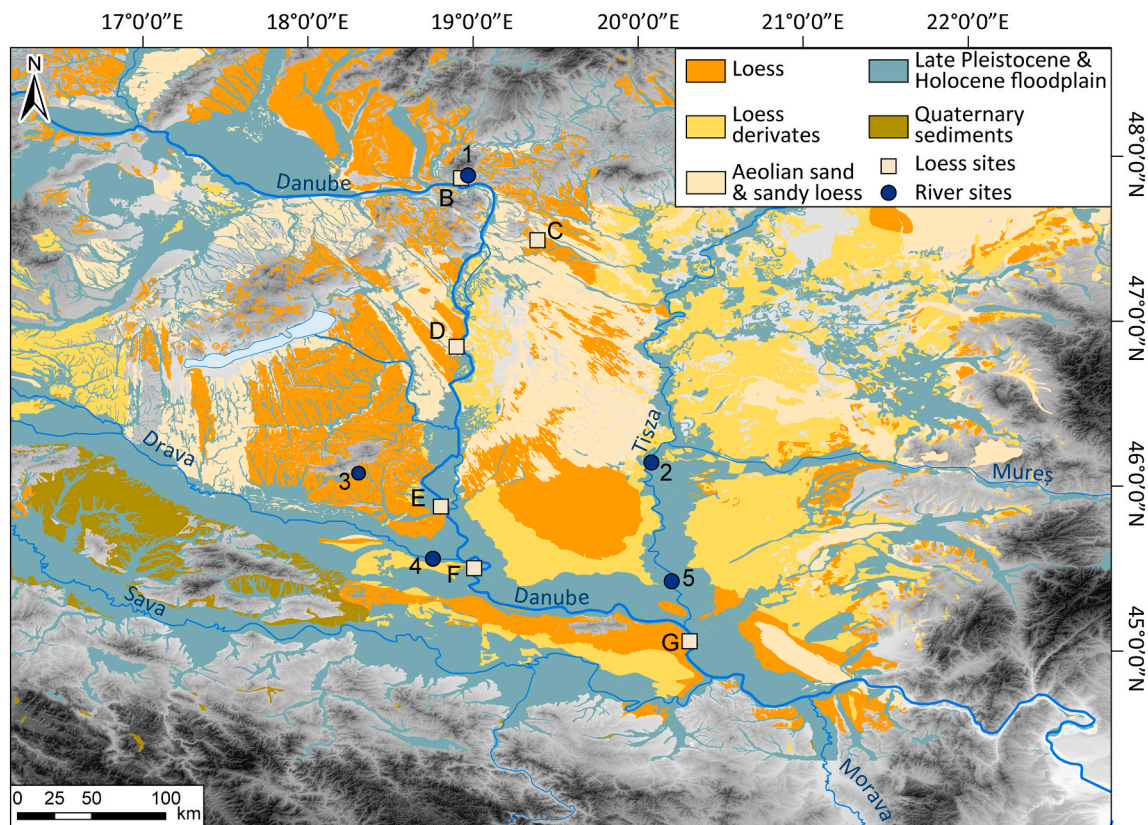


Fig. 9. Distribution of the Quaternary deposits in the Pannonian Basin and the location of the loess and fluvial sites. Capital letters refer to loess profiles B – Basaharc, C – Mende, D – Paks, E – Zmajevac, F – Erdut, G – Surduk 2. Numbers refer to river sites: 1 – Basaharc fluvial sands, 2 – Tisza, 3 – Danita puszta fluvial sands, 4 – Drava, 5 – Tisza. Sedimentary cover geodata source [Lehmkuhl et al. \(2018\)](#).

interglacial setting transport and in most cases tend to comprise small contributions in terms of volume. Consideration also has to be given to the hydraulic sorting as a result of particle density. [Aarons et al. \(2013\)](#) showed that $30\ \mu\text{m}$ zircon dominated fractions will be only transported for $500\ \text{km}$ under $11\ \text{km h}^{-1}$ winds, and would require wind velocities of $29\ \text{km h}^{-1}$ and $43\ \text{km h}^{-1}$ to travel $1000\ \text{km}$ and $2000\ \text{km}$, respectively. These values are also approximate calculations of [Tsoar and Pye \(1987\)](#) which also suggested a need for hurricane strength winds to transport large proportion of grains larger than $20\ \mu\text{m}$ over $1000\ \text{km}$. Given that zircons analysed in this study are larger than $20\text{--}25\ \mu\text{m}$ and the distance between Pannonian Basin and the north African coast is $1400\text{--}1600\ \text{km}$, it is extremely unlikely that far-travelled North African material is a meaningful source of zircons for the Danubian loess. Especially as this research demonstrated that a number of local sources were active during the last glacial period, and would have overwhelmed any long-range coarse particle contributions. However this dataset cannot resolve potential Saharan contributions of grains $< 20\ \mu\text{m}$ and lighter mineral fractions to Quaternary archives in the Pannonian Basin and vicinity, such as palaeosols ([Varga et al., 2013, 2016](#)) and peat bogs ([Longman et al., 2017](#)), and a Saharan dust source to fine grained silt and clay fractions remains plausible. Overall though the simplest explanation for the source of medium and coarse silt size zircons in loess is the drainage area of the Danube River.

5.3. Spatial variability of provenance signal along the Danube

In addition to constraining the distributions of source regions, the MDS map ([Fig. 7](#)) outlines the relationship between individual loess sites. The proximity of all loess sites to the Lower Danube River sample ([Fig. 1](#), points 9, 10, and 12) and its tributaries further supports the conclusion that loess profiles inherit U-Pb age signatures of the adjacent

river material. The MDS plot inset shows small differences in provenance between loess sites, however any variability noted is smaller than that between rivers, and much smaller than that of sources, suggesting no substantial source change between sites.

Nonetheless, the [Fig. 7](#) inset shows some possible very small-scale differences between sites. The partition of Basaharc, Paks, Mende, and Zmajevac from the sites investigated in this study is likely an artefact of sample size differences, and all loess sites could actually belong to a single group. However these four sites are located in the upper parts of the Pannonian Basin above any major tributary confluences ([Fig. 1](#)) and have a reduced zircon U-Pb $600\ \text{Ma}$ population. These loess sites are also separated from the sites investigated in this study by the confluence of the Drava with the Danube ([Fig. 3](#)), which has a relatively large $600\ \text{Ma}$ peak ([Fig. 6](#)). This could suggest that in the upper part of the Pannonian Basin the $600\ \text{Ma}$ grains are suppressed in loess by the younger grains contributed by e.g. Carpathians. If so the Drava would have an important role in refreshing the Proterozoic age grains in the Danubian sediments.

The separation of two Bulgarian sites, Slivata 1 and Slivata 2, on the MDS plot ([Fig. 7](#)), is noteworthy. While the two profiles do not cover the same time interval, the differences seen are linked to increased proportions of grains in the $300\text{--}350\ \text{Ma}$, $500\ \text{Ma}$, and $600\text{--}650\ \text{Ma}$ populations at Slivata 2, whereas larger contributions of Neoproterozoic and Mesoproterozoic grains are seen at Slivata 1 ([Fig. 3](#)). Despite this, it is important to stress that for the most part distributions are very similar suggesting a dominant common source. However the differences could indicate local sources are periodically being activated (reflecting for example the impact of rapid hydroclimate shift) and/or diluting the dominant with the Danubian signal. Although Neoproterozoic and Cambrian outcrops are relatively sparse in the lower Danube, [Haydoutov \(1989\)](#) and [Haydoutov and Yanev \(1997\)](#) describe Cambrian

island-arcs in the Balkan Mountains that are dated to 563 ± 5 Ma (Savov et al., 2001) and 527 ± 18 Ma (Plissart et al., 2012). Sediments derived from these areas are likely delivered via smaller tributaries draining the Balkan Mountains (Fig. 1) and delivering sediment to the vicinity of the loess profiles bordering the Danube River valley.

Plotting the ϵ_{Hf} isotopic for each individual site (Supplementary Fig. S4) and combining it with source data (Fig. 10) suggests only very subtle differences between datasets, e.g. a wide spread of 600 Ma ϵ_{Hf} values is observed for both Slivata profiles; Slivata 2 (Marine Isotope Stage (MIS) 3–5) has a larger positive ϵ_{Hf} cluster whereas at Slivata 1 (MIS 1–2) the dominant hot spot is negative. This could potentially be attributed to dilution of the Danubian signal (and sediment sourced from upstream of the Iron Gates) by contributions from the local rocks as described above. However without further research and complementary provenance techniques it is not possible to resolve these small

differences and identify the driver of the difference between Slivata 1 and Slivata 2.

Surduk 2 loess profile shows a population of young zircons (< 100 Ma; Fig. 3) which overlaps with the Central Srednogorie (Balkan), and a range of Dinaric datasets (Fig. 10). These datasets are also contiguous with small populations in both Slivata datasets, e.g. Dinarides and Srednogorie with Slivata 2. Whilst Srednogorie cannot be the source of sediment for Surduk 2, given its geographical location, it was part of the magmatic arc that stretched from the modern Balkan Mountains into the Southern Carpathians (including parts of the Apuseni, Banat, Timok, and Srednogorie Mountains (Gallhofer et al., 2015)). Hf isotope data are not available for the whole arc, but the timing and magmatic conditions were consistent, and therefore Srednogorie could be a proxy for the whole arc. Consequently, the young zircon grains in Surduk 2 and Slivata could have originated from this arc, and been delivered via Tisza

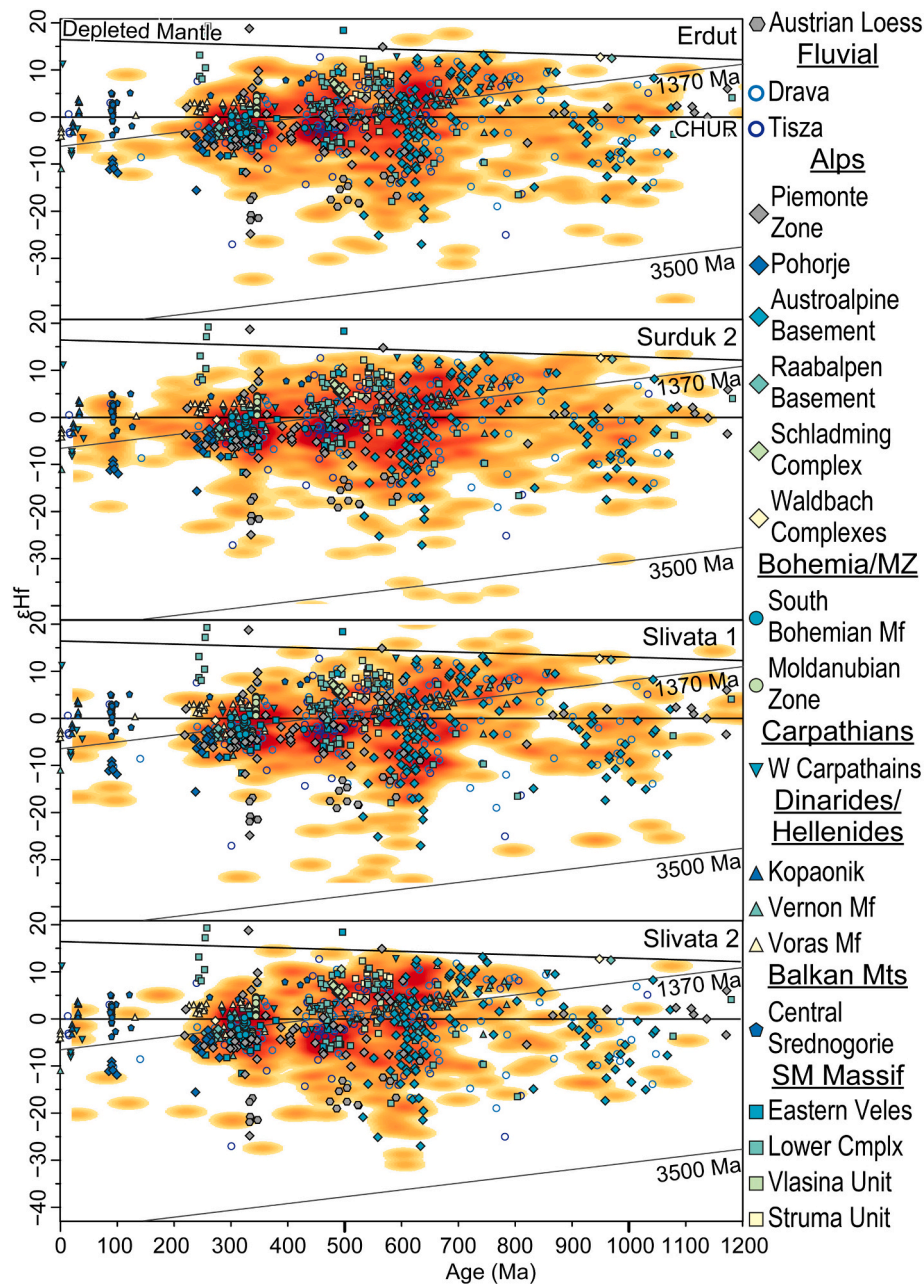


Fig. 10. Probability density plot showing Hf isotope–time evolution for each site for 0–1200 Ma period. Source regions are grouped geographically. The density of the data distribution is calculated using a modified version of the Kernel Density Estimation (Botev et al., 2010) analysis amended for R. ϵ_{Hf} evolution lines for the 1370 Ma and 3500 Ma crust are added. The source of Hf isotope data are superimposed. See Supplementary Table S2 for the Hf isotope metadata.

and small tributaries draining the Balkan Mountains, towards the southern Pannonian Basin.

There is generally limited evidence for significant spatial source variability between loess-palaeosol sites along the Danube River, and mixed sources provide sediment to the wider Pannonian Basin. Further, the main sources remain the same along the Danube River, and therefore support a homogeneous source across the Pannonian Basin model in line with results from studies of bulk sample elemental composition (Buggle et al., 2008; Újvári et al., 2008) and isotopic variation (Schatz et al., 2015). However, small but fairly distinct deviations can be noted in both proxies that indicate variations in source rocks, as previously observed by Újvári and Klötzli (2015) in Austria, and by Újvári et al. (2010) in Hungary and Serbia (Pannonian Basin). These small source changes do not appear to be influenced by gradual additions from the Danube's large tributaries, but most likely result from contributions of smaller sources and local geologies via much shorter pathways, either fluvial or aeolian, that may not be fully captured by the collected datasets. However, as demonstrated, source rocks along the Danube have very similar source signatures and it may not be possible to detect "a step change" with each tributary.

5.4. Implications for loess genesis

A debate on the production mechanism and genesis of loess has long persisted in the literature, and resulted in the primary division of mechanisms into "glacial"/"cold" loess, and "desert"/"warm" loess (Crouvi et al., 2010; Lancaster, 2020; Muhs and Bettis, 2003; Obruchev, 1945; Smalley, 1966; Smalley and Vita-Finzi, 1968; Smith et al., 1991; Tsoar and Pye, 1987; Wright, 2001). Additionally terms such as "mountain" loess also appear in the literature (Jipa, 2014; Smalley, 2008; Smalley et al., 2019; Smalley and Derbyshire, 1990; Xia et al., 2020), especially in relation to desert loess. However, in many cases glacial loess is also ultimately sourced from mountain areas and when production mechanisms (rather than geomorphic areas) are scrutinised the divisions between these categories become rather blurred (Fig. 11).

Glacial grinding has been suggested to be critical for the generation

of large quantities of silt-size sediment for loess (Adamson et al., 2014; Herman et al., 2013; Herman and Champagnac, 2016; Mahaney and Andres, 1991; Wright, 1995, 2001), owing to the fact that loess is typically investigated in the context of glacial periods and Quaternary. However, some researchers have shown that loess can form in the absence of glaciers (Iriondo, 1999; Iriondo and Kröhling, 2007; Soreghan et al., 2008). In the case of Danubian loess, this study demonstrates an absence of a single dominant source supplying sediment to the loess-palaeosol profiles. Instead a number of loess detrital zircon age populations are sourced from an amalgamation of the different geological units along the Danube and surrounding the Pannonian Basin, including the Alps, Carpathians, Dinarides, and Balkan Mountains. During the LGM only the Alps were covered by an ice-cap (Hughes and Woodward, 2017), whilst the other areas supported only smaller, often disconnected, glacier lobes (Engel et al., 2017; Hughes et al., 2011; Klapýta et al., 2021; Sarıkaya et al., 2020; Urdea et al., 2011). This indicates that either the small glaciers are as efficient sediment generator as ice-caps and/or other, mechanisms in mountainous regions such as comminution (fluvial and colluvial), aeolian abrasion, and weathering (physical and chemical), are as important, at least in the Danube region.

Particle comminution during fluvial and colluvial processes has long been suggested as an effective silt generation mechanism (Peng et al., 2016; Smith et al., 2002; Soreghan et al., 2016; Sun, 2002; Wolf et al., 2019; Wright, 2001; Wright et al., 1998). Particle breakdown during fluvial transport is most effective in cases of high energy systems with a high volume of sediment (Smith et al., 2002) and therefore not tied to hot or cold environments. However, it has been argued that in some cases comminution may not be an effective method of silt production, e. g. Wright and Smith (1993) or Pfeifer et al. (2020), and therefore locality and bedrock dependent. Further, rivers can easily erode, transport, and deposit material from sedimentary units and colluvial deposits (Wright, 1995) in a series of cycles. For example, Scherler et al. (2015) demonstrated that periglacial weathering and periodic release of hill-slope sediments into the fluvial system was sufficient for river aggradation. Therefore, fluvial reworking of alluvial and colluvial material could be an important source of silt size sediment.

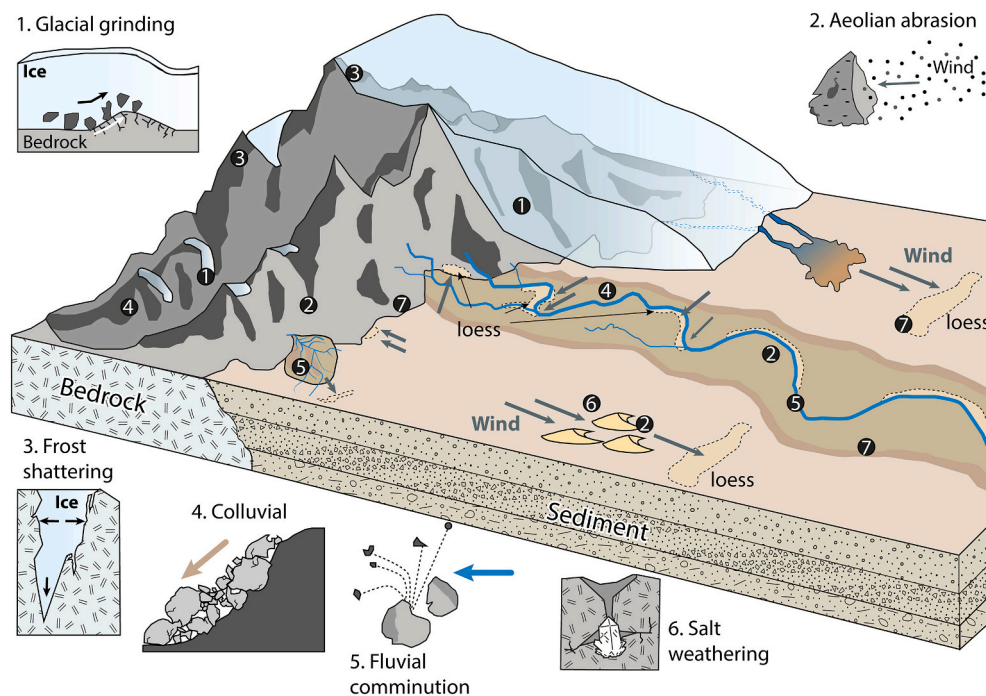


Fig. 11. Schematic illustrating key silt generation mechanisms. Numbers on the schematic refer to the sediment generation processes 1. Glacial grinding; 2. Aeolian abrasion; 3. Frost shattering; 4. Colluvial processes (including grinding and comminution); 5. Fluvial comminution; 6. Salt weathering; 7. Chemical weathering. Please note that the position of loess deposits is purely illustrative and not indicating association with particular features of rivers, alluvial fans, deserts, etc.

Frost shattering and salt weathering are thought to be two of the most effective physical weathering mechanisms of silt generation, though insolation and stress related weathering can also contribute to silt-size particles (Wright, 2007). Whilst frost shattering can occur in a range of environments, sediment generation will be more pronounced when it is acting in combination with glaciers and permafrost, and therefore the process will be most effective in the high mountain and periglacial environments (Derbyshire and Owen, 2018; Rengers et al., 2020; Wright et al., 1998). In fact, Lehmann et al. (2020) recently showed that in previously glaciated Alpine valleys, postglacial erosion, through processes such as frost shattering, can potentially generate relatively large quantities of material. Salt weathering will be the dominant process of mechanical rock breakdown in hot and arid environments (Cilek, 2001; Pavelić et al., 2016; Pye and Sperling, 1983; Smith et al., 2002), though it can still contribute silt-size grains in mountain environments (Sun, 2002). Whilst not typically associated with silt-size particle generation, e.g. (Wright, 2007) and Zan et al. (2020) argued that in cool to temperate climates, weathering profiles can also be an effective production mechanisms. This is further evidenced by Strømsoe and Paasche (2011) who showed chemical weathering is important in the production of grains smaller than 32 µm even in high latitudes.

Comminution and abrasion during aeolian transport are the most contested in terms of their potential for silt-size particle generation, with many arguing that this is an inefficient mechanism. Still, recent laboratory experiments (Bristow and Moller, 2018) show that (mineralogy dependent) auto-abrasion can be sufficient to produce dust material in deserts. Importantly, these processes are unlikely to be operating alone or in isolation, and is likely that the importance of each production mechanism varies along the transport pathway, depending on the type of geomorphic agent, underlying substrate, maturity of sediment, mineralogy, topography, climate, stage of weathering, etc.

The results of the zircon U-Pb and Hf isotope analyses presented here provide additional field evidence that the two models of cold versus warm loess are unnecessary and only result in a false dichotomy. Most silt-generation processes can operate in desert/glacial regions and silt size sediment is likely to be produced and transported by various mechanisms simultaneously. Consequently the authors support the growing body of literature that advocates for the use of the following terminology in relation to loess genesis; continental glacier provenance-river transport, mountain provenance-river transport, and mountain provenance-river transport-desert transition (Li et al., 2020).

5.5. Approaches to loess provenance

A number of loess provenance studies (e.g. Licht et al., 2016; Pullen et al., 2014) have been published over the last few years that rely exclusively on zircon U-Pb data and argue that by increasing the number of grains analysed, specific sources can be identified. While this approach can be powerful in some loess provenance settings, if two different sources are contributing grains of the same age (as seen in this research), then increasing the number of analyses will not aid in distinguishing between two similar-age signals. Several authors have shown (Bird et al., 2015; Fenn et al., 2018; Stevens et al., 2013) that relying on zircon U-Pb ages alone cannot resolve sources for loess sedimentary settings with complex source rock relationships, and call for more multi-proxy provenance approaches. This study showcases Hf isotopic composition of zircons as a powerful tool for understanding loess provenance in a case where several sources have similar ages. Investigating Hf isotopes in zircons seems a natural next step as grains used for U-Pb analysis can be re-analysed, saving time on sample preparation and grain extraction and allowing two provenance indicators to be derived from one grain. However, more work is needed by loess provenance researchers to combine single grain analyses with bulk sample, petrographic, and other single minerals grain approaches, as seen in some other sedimentary provenance communities (e.g. Fielding

et al., 2017, 2018; Pastore et al., 2021; Vermeesch and Garzanti, 2015; Zhang et al., 2019). Whilst some attempts already have been made by loess researchers e.g. bulk sample Nd, Sr, and Hf analyses (Bird et al., 2020; Újvári et al., 2012), rutile geochemistry (Újvári et al., 2013), mineral assemblages (Nie et al., 2015; Stevens et al., 2013), and garnet analysis (Fenn et al., 2018), these need to become the norm. A first step should be focused on combining single grain studies with the wealth of bulk sample elemental composition data that is available for loess profiles (Bosq et al., 2020; Buggle et al., 2008; Hao et al., 2010; Skurzyński et al., 2020; Újvári et al., 2014; Varga et al., 2011).

6. Conclusions

This study presents the findings of the provenance investigation, using zircon U-Pb dating and Hf isotopes, of loess-palaeosol deposits along the middle and lower reaches of the Danube River. Loess in the region does not have a single dominant origin but is rather sourced from different areas (the Alps, the Bohemian Massif, the Carpathians, the Dinarides, and the Balkan Mountains) along the Danube valley, and is well mixed in the Danube itself. The first detailed application of zircon Hf isotopes in loess deposits suggests that metasedimentary rocks of the Austroalpine basement in the Alps may represent a large sediment contributor. The Dinaric and Balkan regions, which have not been investigated in the past as a sediment source, were also shown to be an active supplier of zircons to loess deposits along the Danube River. This has implications for our understanding of loess generation as these latter regions were not extensively glaciated during the last glacial period and therefore other sediment generation mechanisms should be investigated. Moreover, in terms of the proximal, geomorphological source, the data point to the Danube's alluvium as the main dust contributor, showing that sediment is mixed during fluvial transport (deposition and recycling) and experiences predominantly short-distance aeolian transport prior to deposition. Lastly, provenance remains mostly unchanged for loess sequences along the Danube and across the Pannonian Basin. However, small additions from other, most likely proximal geologies, can be seen at some sites.

Declaration of Competing Interest

The authors declare that they have no known competing financial interests or personal relationships that could have appeared to influence the work reported in this paper.

Acknowledgements

This research was funded by the UK Natural Environmental Research Council (grant: NE/L002612/1), NIGL Natural Environmental Research Council grant, International Association of Sedimentologists Postgraduate Research Grants, and Hertford College Travel Fund. TS acknowledges the support of the Swedish Research Council for research into European loess sources (project 220017-03888). We are grateful to Nemanja Tomić and Zoran Perić for the assistance in the field. The lead author is also grateful to WHWR for the mental support during COVID and to Dr. Kirstie Wright for all discussions regarding geology of Europe.

Appendix A. Supplementary data

Supplementary data to this article can be found online at <https://doi.org/10.1016/j.earscirev.2022.103920>.

References

- Aarons, S.M., Aciego, S.M., Gleason, J.D., 2013. Variable Hf-Sr-Nd radiogenic isotopic compositions in a Saharan dust storm over the Atlantic: Implications for dust flux to oceans, ice sheets and the terrestrial biosphere. *Chem. Geol.* 349–350, 18–26. <https://doi.org/10.1016/j.chemgeo.2013.04.010>.

- Abbo, A., Avigad, D., Gerdes, A., 2018. The lower crust of the Northern broken edge of Gondwana: evidence for sediment subduction and syn-Variscan anorogenic imprint from zircon U-Pb-Hf in granulite xenoliths. *Gondwana Res.* 64, 84–96. <https://doi.org/10.1016/j.gr.2018.08.002>.
- Abbo, A., Avigad, D., Gerdes, A., 2020. Crustal evolution of peri-Gondwana crust into present day Europe: the Serbo-Macedonian and Rhodope massifs as a case study. *Lithos* 356–357, 105295. <https://doi.org/10.1016/j.lithos.2019.105295>.
- Adamson, K.R., Woodward, J.C., Hughes, P.D., 2014. Glacial crushing of limestone and the production of carbonate-rich silts in a pleistocene glaciofluvial system: a potential source of loess in southern Europe. *Geogr. Ann. Ser. A Phys. Geogr.* 96, 339–356. <https://doi.org/10.1111/geoa.12054>.
- Antić, M., Peytcheva, I., von Quadt, A., Kounov, A., Trivić, B., Serafimovski, T., Tasev, G., Gerđjkov, I., Wetzel, A., 2016. Pre-Alpine evolution of a segment of the North-Gondwanan margin: geochronological and geochemical evidence from the central Serbo-Macedonian Massif. *Gondwana Res.* 36, 523–544. <https://doi.org/10.1016/j.gr.2015.07.020>.
- Antoine, P., Rousseau, D.-D., Fuchs, M., Hatté, C., Gauthier, C., Marković, S.B., Jovanović, M., Gaudenyi, T., Moine, O., Rossignol, J., 2009. High-resolution record of the last climatic cycle in the southern Carpathian Basin (Surduk, Vojvodina, Serbia). *Quat. Int.* 198, 19–36. <https://doi.org/10.1016/j.quaint.2008.12.008>.
- Antoine, P., Lagroix, F., Jordanova, D., Jordanova, N., Lomax, J., Fuchs, M., Debret, M., Rousseau, D.-D., Hatté, C., Gauthier, C., Moine, O., Taylor, S.N., Till, J.L., Coutard, S., 2019. A remarkable late Saalian (MIS 6) loess (dust) accumulation in the lower Danube at Harletz (Bulgaria). *Quat. Sci. Rev.* 207, 80–100. <https://doi.org/10.1016/j.quascirev.2019.01.005>.
- Avigad, D., Morag, N., Abbo, A., Gerdes, A., 2017. Detrital rutile U-Pb perspective on the origin of the great Cambro-Ordovician sandstone of North Gondwana and its linkage to orogeny. *Gondwana Res.* 51, 17–29. <https://doi.org/10.1016/j.gr.2017.07.001>.
- Badura, J., Jary, Z., Smalley, I.J., 2013. Sources of loess material for deposits in Poland and parts of Central Europe: The lost Big River. *Quat. Int.* 296, 15–22. <https://doi.org/10.1016/j.quaint.2012.06.019>.
- Bagnold, R.A., 1941. *The Physics of Blown Sand and Desert Dunes*. Methuen, London.
- Balintoni, I., Balica, C., Ducea, M.N., Hann, H.P., 2014. Peri-Gondwanan terranes in the Romanian Carpathians: a review of their spatial distribution, origin, provenance, and evolution. *Geosci. Front.* 5, 395–411. <https://doi.org/10.1016/j.gsf.2013.09.002>.
- Banak, A., Mandić, O., Kovačić, M., Pavelić, D., 2012. Late Pleistocene climate history of the Baranja loess plateau – evidence from the Zmajevac loess-paleosol section (northeastern Croatia). *Geol. Croat.* 65, 411–422. <https://doi.org/10.4154/gc.2013.05>.
- Banak, A., Pavelić, D., Kovačić, M., Mandić, O., 2013. Sedimentary characteristics and source of loess in Baranja (Eastern Croatia). *Aeolian Res.* 11, 129–139. <https://doi.org/10.1016/j.aeolia.2013.08.002>.
- Basarin, B., Vandenbergh, D.A.G., Marković, S.B., Catto, N., Hambach, U., Vasiliniuc, S., Derese, C., Rončević, S., Vasiljević, D.A., Rajić, L., 2011. The Belotinac section (Southern Serbia) at the southern limit of the European loess belt: initial results. *Quat. Int.* 240, 128–138. <https://doi.org/10.1016/j.quaint.2011.02.022>.
- Baykal, Y., Stevens, T., Engström-Johansson, A., Skurzyński, J., Zhang, H., He, J., Adamiec, G., Kólringer, C., Jary, Z., 2021. Detrital zircon U-Pb age analysis of last glacial loess sources and proglacial sediment dynamics in the Northern European Plain. *Quat. Sci. Rev.* 274. <https://doi.org/10.1016/j.quascirev.2021.107265>.
- Bird, A.F., Stevens, T., Rittner, M., Vermeesch, P., Carter, A., Andò, S., Garzanti, E., Lu, H., Nie, J., Zeng, L., Zhang, H., Xu, Z., 2015. Quaternary dust source variation across the Chinese Loess Plateau. *Palaeogeogr. Palaeoclimatol. Palaeoecol.* 435, 254–264. <https://doi.org/10.1016/j.palaeo.2015.06.024>.
- Bird, A.F., Millar, I.L., Rodenburg, T., Stevens, T., Rittner, M., Vermeesch, P., Lu, H., 2020. A constant Chinese Loess Plateau dust source since the late Miocene. *Quat. Sci. Rev.* 227, 106042. <https://doi.org/10.1016/j.quascirev.2019.106042>.
- Blichert-Toft, J., 2008. The Hf isotopic composition of zircon reference material 91500. *Chem. Geol.* 253, 252–257. <https://doi.org/10.1016/j.chemgeo.2008.05.014>.
- Bogdanova, S.V., Gorbatshev, R., Grad, M., Janik, T., Guterch, A., Kozlovskaya, E., Motuza, G., Skridlaite, G., Starostenko, V., Taran, L., Group, E.W., Group, P.W., 2006. EUROBRIDGE: new insight into the geodynamic evolution of the East European Craton. *Geol. Soc. Mem.* 32, 599–625.
- Bogdanova, S.V., Bingen, B., Gorbatshev, R., Kheraskova, T.N., Kozlov, V.I., Puchkov, V. N., Volozh, Y.A., 2008. The east European Craton (Baltica) before and during the assembly of Rodinia. *Precambrian Res.* 160, 23–45. <https://doi.org/10.1016/j.precamres.2007.04.024>.
- Bokhorst, M.P., Vandenbergh, J., Sümeği, P., Lanczont, M., Gerasimenko, N.P., Matviishina, Z.N., Marković, S.B., Frechen, M., 2011. Atmospheric circulation patterns in central and eastern Europe during the Weichselian Pleniglacial inferred from loess grain-size records. *Quat. Int.* 234, 62–74. <https://doi.org/10.1016/j.quaint.2010.07.018>.
- Bösken, J., Obrecht, I., Zeeden, C., Klasen, N., Hambach, U., Sümeği, P., Lehmkuhl, F., 2019. High-resolution paleoclimatic proxy data from the MIS3/2 transition recorded in northeastern Hungarian loess. *Quat. Int.* 502, 95–107. <https://doi.org/10.1016/j.quaint.2017.12.008>.
- Bosq, M., Bertran, P., Degeai, J.P., Que, A., Moine, O., 2020. Geochemical signature of sources, recycling and weathering in the last Glacial loess from the Rhône Valley (Southeast France) and comparison with other European regions. *Aeolian Res.* 42, 100561. <https://doi.org/10.1016/j.aeolia.2019.100561>.
- Botev, Z.I., Grotowski, J.F., Kroese, D.P., 2010. Kernel density estimation via diffusion. *Ann. Stat.* 38, 2916–2957. <https://doi.org/10.1214/10-AOS799>.
- Bouvier, A., Vervoort, J.D., Patchett, P.J., 2008. The Lu-Hf and Sm-Nd isotopic composition of CHUR: Constraints from unequilibrated chondrites and implications for the bulk composition of terrestrial planets. *Earth Planet. Sci. Lett.* 273, 48–57. <https://doi.org/10.1016/j.epsl.2008.06.010>.
- Bristow, C.S., Moller, T.H., 2018. Testing the auto-abrasion hypothesis for dust production using diatomite dune sediments from the Bodélé Depression in Chad. *Sedimentology* 65, 1322–1330. <https://doi.org/10.1111/sed.12423>.
- Buggle, B., Glaser, B., Zöller, L., Hambach, U., Marković, S.B., Glaser, I., Gerasimenko, N. P., 2008. Geochemical characterization and origin of Southeastern and Eastern European loesses (Serbia, Romania, Ukraine). *Quat. Sci. Rev.* 27, 1058–1075. <https://doi.org/10.1016/j.quascirev.2008.01.018>.
- Bullard, J.E., 2013. Contemporary glacial inputs to the dust cycle. *Earth Surf. Process. Landf.* 38, 71–89. <https://doi.org/10.1002/esp.3315>.
- Burda, J., Klötzli, U.S., Majka, J., Chew, D.M., Li, Q.L., Liu, Y., Gawęda, A., Wiedenbeck, M., 2021. Tracing proto-Rheic - Qaidam Ocean vestiges into the Western Tatra Mountains and implications for the Palaeozoic palaeogeography of Central Europe. *Gondwana Res.* 91, 188–204. <https://doi.org/10.1016/j.gr.2020.12.016>.
- Cawood, P.A., Buchan, C., 2007. Linking accretionary orogenesis with supercontinent assembly. *Earth-Sci. Rev.* 82, 217–256. <https://doi.org/10.1016/j.earscirev.2007.03.003>.
- Che, X., Li, G., 2013. Binary sources of loess on the Chinese Loess Plateau revealed by U-Pb ages of zircon. *Quat. Res.* 80, 545–551. <https://doi.org/10.1016/j.yqres.2013.05.007>.
- Chen, F., Todt, W., Hann, H.P., 2003. Zircon and garnet geochronology of eclogites from the Moldanubian zone of the Black Forest, Germany. *J. Geol.* 111, 207–222.
- Cilek, V., 2001. The loess deposits of the Bohemian Massif: Silt provenance, palaeometeorology and loessification processes. *Quat. Int.* 76–77, 123–128. [https://doi.org/10.1016/S1040-6182\(00\)00096-3](https://doi.org/10.1016/S1040-6182(00)00096-3).
- Crouvi, O., Amit, R., Enzel, Y., Gillespie, A.R., 2010. Active sand seas and the formation of desert loess. *Quat. Sci. Rev.* 29, 2087–2098. <https://doi.org/10.1016/j.quascirev.2010.04.026>.
- Da Silva, L.C., McNaughton, N.J., Armstrong, R., Hartmann, L.A., Fletcher, I.R., 2005. The neoproterozoic Mantiqueira Province and its African connections: a zircon-based U-Pb geochronologic subdivision for the Brasiliano/Pan-African systems of orogens. *Precambrian Res.* 136, 203–240. <https://doi.org/10.1016/j.precamres.2004.10.004>.
- Derbyshire, E., Owen, L.A., 2018. Glacioaeolian processes, sediments, and landforms. In: *Past Glacial Environments*. Elsevier Ltd, pp. 273–308. <https://doi.org/10.1016/B978-0-08-100524-8.00008-7>.
- Derbyshire, E., Meng, X., Kemp, R.A., 1998. Provenance, transport and characteristics of modern aeolian dust in western Gansu Province, China, and interpretation of the Quaternary loess record. *J. Arid Environ.* 39, 497–516. <https://doi.org/10.1006/jare.1997.0369>.
- Ducea, M.N., Giosan, L., Carter, A., Balica, C., Stoica, A.M., Roban, R.D., Balintoni, I., Filip, F., Petrescu, L., 2018. U-Pb detrital zircon geochronology of the lower danube and its tributaries: implications for the geology of the carpathians. *Geochim. Geophys. Geosyst.* 19, 3208–3223. <https://doi.org/10.1029/2018GC007659>.
- Edel, J.B., Schulmann, K., Lexa, O., Lardeaux, J.M., 2018. Late Palaeozoic palaeomagnetic and tectonic constraints for amalgamation of Pangea supercontinent in the European Variscan belt. *Earth-Sci. Rev.* 177, 589–612. <https://doi.org/10.1016/j.earscirev.2017.12.007>.
- Engel, Z., Krížek, M., Kasprzak, M., Traczyk, A., Hložek, M., Krbcová, K., 2017. Geomorphological and sedimentary evidence of probable glaciation in the Jizerské hory Mountains, Central Europe. *Geomorphology* 280, 39–50. <https://doi.org/10.1016/j.geomorph.2016.12.008>.
- Fenn, K., Stevens, T., Bird, A.F., Limonta, M., Rittner, M., Vermeesch, P., Andò, S., Garzanti, E., Lu, H., Zhang, H., Lin, Z., 2018. Insights into the provenance of the Chinese Loess Plateau from joint zircon U-Pb and garnet geochemical analysis of last glacial loess. *Quat. Res.* 89. <https://doi.org/10.1017/qua.2017.86>.
- Fenn, K., Durcan, J.A., Thomas, D.S.G., Banak, A., 2020a. A 180 ka record of environmental change at Erdut (Croatia): a new chronology for the loess-paleosol sequence and its implications for environmental interpretation. *J. Quat. Sci.* 35, 582–593. <https://doi.org/10.1002/jqs.3201>.
- Fenn, K., Durcan, J.A., Thomas, D.S.G., Millar, I.L., Marković, S.B., 2020b. Re-analysis of late Quaternary dust mass accumulation rates in Serbia using new luminescence chronology for loess-paleosol sequence at Surduk. *Boreas* 49, 634–652. <https://doi.org/10.1111/bor.12445>.
- Fenn, K., Thomas, D.S.G., Durcan, J.A., Millar, I.L., Veres, D., Piermattei, A., Lane, C.S., 2021. A tale of two signals: global and local in fl uences on the Late Pleistocene loess sequences in Bulgarian Lower Danube. *Quat. Sci. Rev.* 274, 107264. <https://doi.org/10.1016/j.quascirev.2021.107264>.
- Fielding, L., Najman, Y., Millar, I.L., Butterworth, P., Ando, S., Padoan, M., Barford, D., Kneller, B., 2017. A detrital record of the Nile River and its catchment. *J. Geol. Soc. Lond.* 174, 301–317. <https://doi.org/10.1144/jgs2016-075>.
- Fielding, L., Najman, Y., Millar, I.L., Butterworth, P., Garzanti, E., Vezzoli, G., Barford, D., Kneller, B., 2018. The initiation and evolution of the River Nile. *Earth Planet. Sci. Lett.* 489, 166–178. <https://doi.org/10.1016/j.epsl.2018.02.031>.
- Friese, C.A., Van Hateren, J.A., Vogt, C., Fischer, G., Stuut, J.-B.W., 2017. Seasonal provenance changes in present-day Saharan dust collected in and off Mauritania. *Atmos. Chem. Phys.* 10163–10193.
- Fukum, C., 2002. Polymetamorphism of the variscan basement of the Moldanubian Black Forest (Germany) documented in Zircon and Garnet minerals from Gneisses. *Chin. J. Geochim.* 21, 107–119.
- Gallhofer, D., Von Quadt, A., Peytcheva, I., Schmid, S.M., Heinrich, C.A., 2015. Tectonic, magmatic, and metallogenic evolution of the Late Cretaceous arc in the Carpathian-Balkan orogen. *Tectonics* 34, 1813–1836. <https://doi.org/10.1002/2015TC003834>.
- Gee, D.G., Ladenberger, A., Dahlqvist, P., Majka, J., Be'eri-Shlevin, Y., Frei, D., Thomsen, T., 2014. The Baltoscandian margin detrital zircon signatures of the

- central scandes. *Geol. Soc. Spec. Publ.* 390, 131–155. <https://doi.org/10.1144/SP390.20>.
- Goudie, A.S., Middleton, N.J., 2001. Saharan dust storms: Nature and consequences. *Earth-Sci. Rev.* 56, 179–204. [https://doi.org/10.1016/S0012-8252\(01\)00067-8](https://doi.org/10.1016/S0012-8252(01)00067-8).
- Griffin, W.L., Pearson, N.J., Belousova, E.A., Saeed, A., 2006. Comment: Hf-isotope heterogeneity in zircon 91500. *Chem. Geol.* 233, 358–363. <https://doi.org/10.1016/j.chemgeo.2006.03.007>.
- Guerzoni, S., Molinaroli, E., Chester, R., 1997. Saharan dust inputs to the western Mediterranean Sea: depositional patterns, geochemistry and sedimentological implications. *Deep. Res. II* 44, 631–654.
- Haas, I., Eichinger, S., Haller, D., Fritz, H., Nievoil, J., Mandl, M., Hippler, D., Hauzenberger, C., 2020. Gondwana fragments in the Eastern Alps: a travel story from U/Pb zircon data South-Alpine. *Gondwana Res.* 77, 204–222. <https://doi.org/10.1016/j.jgr.2019.07.015>.
- Hao, Q., Guo, Z., Qiao, Y., Xu, B., Oldfield, F., 2010. Geochemical evidence for the provenance of middle Pleistocene loess deposits in southern China. *Quat. Sci. Rev.* 29, 3317–3326. <https://doi.org/10.1016/j.quascirev.2010.08.004>.
- Haydoutov, I., 1989. Precambrian ophiolites, Cambrian island arc, and Variscan suture in the South Carpathian-Balkan region. *Geology* 17, 905–908. [https://doi.org/10.1130/0091-7613\(1989\)017<0905:POCIAA>2.3.CO;2](https://doi.org/10.1130/0091-7613(1989)017<0905:POCIAA>2.3.CO;2).
- Haydoutov, I., Yanev, S., 1997. The Protomoesian microcontinent of the Balkan Peninsula - a peri-Gondwanaland piece. *Tectonophysics* 272, 303–313. [https://doi.org/10.1016/S0040-1951\(96\)00264-8](https://doi.org/10.1016/S0040-1951(96)00264-8).
- Hefferan, K., Soulaïmani, A., Samson, S.D., Admou, H., Inglis, J., Saquaque, A., Latifa, C., Heywood, N., 2014. A reconsideration of Pan African orogenic cycle in the Anti-Atlas Mountains, Morocco. *J. Afr. Earth Sci.* 98, 34–46. <https://doi.org/10.1016/j.jafrearsci.2014.03.007>.
- Herman, F., Champagnac, J.D., 2016. Plio-Pleistocene increase of erosion rates in mountain belts in response to climate change. *Terra Nova* 28, 2–10. <https://doi.org/10.1111/ter.12186>.
- Herman, F., Seward, D., Valla, P.G., Carter, A., Kohn, B., Willett, S.D., Ehlers, T.A., 2013. Worldwide acceleration of mountain erosion under a cooling climate. *Nature* 504, 423–426. <https://doi.org/10.1038/nature12877>.
- Horstwood, M.S.A., Köslér, J., Gehrels, G.E., Jackson, S.E., McLean, N.M., Paton, C., Pearson, N.J., Sircombe, K.N., Sylvester, P., Vermeesch, P., Bowring, J.F., Condon, D. J., Schoene, B., 2016. Community-Derived Standards for LA-ICP-MS U-(Th)-Pb Geochronology – uncertainty Propagation, Age Interpretation and Data Reporting. *Geostand. Geoanal. Res.* 40, 311–332. <https://doi.org/10.1111/j.1751-908X.2016.00379.x>.
- Huang, Q., Genser, J., Liu, Y., Neubauer, F., Yuan, S., Bernroider, M., Guan, Q., Jin, W., Yu, S., Chang, R., 2021. Cambrian-Ordovician continental magmatic arc at the northern margin of Gondwana: Insights from the Schlading complex. *Eastern Alps. Lithos* 388–389. <https://doi.org/10.1016/j.lithos.2021.106064>.
- Hughes, P.D., Woodward, J.C., 2017. Quaternary glaciation in the Mediterranean mountains: a new synthesis. *Geol. Soc. Spec. Publ.* 433, 1–23. <https://doi.org/10.1144/SP433.14>.
- Hughes, P.D., Woodward, J.C., van Calsteren, P.C., Thomas, L.E., 2011. The glacial history of the Dinaric Alps, Montenegro. *Quat. Sci. Rev.* 30, 3393–3412. <https://doi.org/10.1016/j.quascirev.2011.08.016>.
- Iizuka, T., Campbell, I.H., Allen, C.M., Gill, J.B., Maruyama, S., Makoka, F., 2013. Evolution of the African continental crust as recorded by U-Pb, Lu-Hf and O isotopes in detrital zircons from modern rivers. *Geochim. Cosmochim. Acta* 107, 96–120. <https://doi.org/10.1016/j.gca.2012.12.028>.
- Iriondo, M., 1999. The origin of silt particles in the loess question. *Quat. Int.* 62, 3–9. [https://doi.org/10.1016/S1040-6182\(99\)00018-X](https://doi.org/10.1016/S1040-6182(99)00018-X).
- Iriondo, M.H., Kröhlhng, D.M., 2007. Non-classical types of loess. *Sediment. Geol.* 202, 352–368. <https://doi.org/10.1016/j.sedgeo.2007.03.012>.
- Jipa, D.C., 2014. The conceptual sedimentary model of the lower Danube loess basin: Sedimentogenetic implications. *Quat. Int.* 351, 14–24. <https://doi.org/10.1016/j.quaint.2013.06.008>.
- Johnson, P.R., Andresen, A., Collins, A.S., Fowler, A.R., Fritz, H., Ghebreab, W., Kusky, T., Stern, R.J., 2011. Late Cryogenian-Ediacaran history of the Arabian-Nubian Shield: a review of depositional, plutonic, structural, and tectonic events in the closing stages of the northern East African Orogen. *J. Afr. Earth Sci.* 61, 167–232. <https://doi.org/10.1016/j.jafrearsci.2011.07.003>.
- Jordanova, D., Hus, J., Evlogiev, J., Geeraerts, R., 2008. Palaeomagnetism of the loess/palaeosol sequence in Viatovo (NE Bulgaria) in the Danube basin. *Phys. Earth Planet. Inter.* 167, 71–83. <https://doi.org/10.1016/j.pepi.2008.02.008>.
- Klapayta, P., Mindrescu, M., Zasadni, J., 2021. Geomorphological record and equilibrium line altitude of glaciers during the last glacial maximum in the Rodna Mountains (eastern Carpathians). *Quat. Res.* 100, 1–20. <https://doi.org/10.1017/qua.2020.90>.
- Kostić, N.S., Protić, N., 2000. Pedology and mineralogy of loess profiles at Kapela-Batajnica and Stalac, Serbia. *Catena* 41, 217–227.
- Kouamelan, A.N., Kra, K.S.A., Djro, S.C., Paquette, J.L., Peucat, J.J., 2018. The Logoué Band: a large Archean crustal block in the Kenema-Man domain (Man-Leo rise, West African Craton) remobilized during Eburnean orogeny (2.05 Ga). *J. Afr. Earth Sci.* 148, 6–13. <https://doi.org/10.1016/j.jafrearsci.2017.09.004>.
- Kristoffersen, M., Andersen, T., Elburg, M.A., Watkeys, M.K., 2016. Detrital zircon in a supercontinental setting: locally derived and far-transported components in the Ordovician Natal Group, South Africa. *J. Geol. Soc. Lond.* 173, 203–215. <https://doi.org/10.1144/jgs2015-012>.
- Kroner, U., Romer, R.L., 2013. Two plates - many subduction zones: the Variscan orogeny reconsidered. *Gondwana Res.* 24, 298–329. <https://doi.org/10.1016/j.gr.2013.03.001>.
- Küster, D., Harms, U., 1998. Post-collisional potassic granitoids from the southern and northwestern parts of the Late Neoproterozoic East African Orogen: a review. *Lithos* 45, 177–195. [https://doi.org/10.1016/S0024-4937\(98\)00031-0](https://doi.org/10.1016/S0024-4937(98)00031-0).
- Lancaster, N., 2020. On the formation of desert loess. *Quat. Res.* 1–18. <https://doi.org/10.1017/qua.2020.33>.
- Lawrence, C.R., Neff, J.C., 2009. The contemporary physical and chemical flux of aeolian dust: a synthesis of direct measurements of dust deposition. *Chem. Geol.* 267, 46–63. <https://doi.org/10.1016/j.chemgeo.2009.02.005>.
- Lehmann, B., Herman, F., Valla, P.G., King, G.E., Biswas, R.H., Ivy-Ochs, S., Steinemann, O., Christl, M., 2020. Postglacial erosion of bedrock surfaces and deglaciation timing: new insights from the Mont Blanc massif (western Alps). *Geology* 48, 139–144. <https://doi.org/10.1130/G46585.1>.
- Lehmkuhl, F., Zens, J., Krauß, L., Schulte, P., Kels, H., 2016. Loess-paleosol sequences at the northern European loess belt in Germany: distribution, geomorphology and stratigraphy. *Quat. Sci. Rev.* 153, 11–30. <https://doi.org/10.1016/j.quascirev.2016.10.008>.
- Lehmkuhl, F., Böskén, J., Hošek, J., Sprafke, T., Marković, S.B., Obrecht, I., Hambach, U., Sümeği, P., Thiemann, A., Steffens, S., Lindner, H., Veres, D., Zeeden, C., 2018. Loess distribution and related Quaternary sediments in the Carpathian Basin. *J. Maps* 14, 661–670. <https://doi.org/10.1080/17445647.2018.1526720>.
- Lehmkuhl, F., Nett, J., Pötter, S., Schulte, P., Sprafke, T., Jary, Z., Antoine, P., Wacha, L., Wolf, D., Zerbini, A., Hošek, J., Marković, S.B., Obrecht, I., Sümeği, P., Veres, D., Zeeden, C., Boemke, B., Schaubert, V., Viehweger, J., Hambach, U., 2021. Loess landscapes of Europe – Mapping, geomorphology, and zonal differentiation. *Earth-Sci. Rev.* 215. <https://doi.org/10.1016/j.earscirev.2020.103496>.
- Li, Y., Shi, W., Aydin, A., Beroya-Eitner, M.A., Gao, G., 2020. Loess genesis and worldwide distribution. *Earth-Sci. Rev.* 201, 102947. <https://doi.org/10.1016/j.earscirev.2019.102947>.
- Licht, A., Pullen, A., Kapp, P., Abell, J., Giesler, N., 2016. Eolian cannibalism: Reworked loess and fluvial sediment as the main sources of the Chinese Loess Plateau. *GSA Bull.* 128, 944–956. <https://doi.org/10.1130/B31375.1>.
- Linnemann, U., Herbolch, A., Liégeois, J.P., Pin, C., Gärtner, A., Hofmann, M., 2012. The Cambrian to Devonian odyssey of the Brabant Massif within Avalonia: a review with new zircon ages, geochemistry, Sm-Nd isotopes, stratigraphy and palaeogeography. *Earth-Sci. Rev.* 112, 126–154. <https://doi.org/10.1016/j.earscirev.2012.02.007>.
- Linnemann, U., Gerdes, A., Hofmann, M., Marko, L., 2014. The Cadomian Orogen: neoproterozoic to early Cambrian crustal growth and orogenic zoning along the periphery of the West African Craton-Constraints from U-Pb zircon ages and Hf isotopes (Schwarzbach Antiform, Germany). *Precambrian Res.* 244, 236–278. <https://doi.org/10.1016/j.precamres.2013.08.007>.
- Longman, J., Veres, D., Ersek, V., Salzmann, U., Hubay, K., Bormann, M., Wennrich, V., Schäbitz, F., 2017. Periodic input of dust over the Eastern Carpathians during the Holocene linked with Saharan desertification and human impact. *Clim. Past* 13, 897–917. <https://doi.org/10.5194/cp-13-897-2017>.
- Lorentzen, S., Augustsson, C., Nystuen, J.P., Berndt, J., Jahren, J., Schovsbo, N.H., 2018. Provenance and sedimentary processes controlling the formation of lower Cambrian quartz arenite along the southwestern margin of Baltica. *Sediment. Geol.* 375, 203–217. <https://doi.org/10.1016/j.sedgeo.2017.08.008>.
- Loth, G., Eichhorn, R., Holl, R., Kennedy, A., Schauder, P., Sollner, F., 2001. Cambro-Ordovician age of a metagabbro from the Wildschönau ophiolite complex, Greywacke Supergroup (Eastern Alps, Austria): a U-Pb SHRIMP study. *Eur. J. Mineral.* 57–66. <https://doi.org/10.1127/0935-1221/01/0013-0057>.
- Mahaney, W.C., Andres, W., 1991. Glacially crushed quartz grains. *Boreas* 20, 231–239.
- Mahowald, N., Albani, S., Kok, J.F., Engelstaedter, S., Scanza, R., Ward, D.S., Flanner, M. G., 2014. The size distribution of desert dust aerosols and its impact on the Earth system. *Aeolian Res.* 15, 53–71. <https://doi.org/10.1016/j.aeolia.2013.09.002>.
- Marković, S.B., Hambach, U., Gaudenyi, T., Jovanović, M., Zöller, L., Machalet, B., Savić, S., Romelić, J., Plavska, J., Mesaros, M., 2006. An introduction to the late Pleistocene loess-paleosol sequence at Susek, Vojvodina, Serbia. *Geogr. Pannonica* 4–8. <https://doi.org/10.5937/geopan0610004m>.
- Marković, S.B., Bokhorst, M.P., Vandenbergh, J., McCoy, W.D., Oches, E.A., Hambach, U., Gaudenyi, T., Jovanović, M., Zöller, L., Stevens, T., Machalet, B., 2008. Late Pleistocene loess-paleosol sequences in the Vojvodina region, North Serbia. *J. Quat. Sci.* 23, 73–84. <https://doi.org/10.1002/jqs>.
- Marković, S.B., Hambach, U., Stevens, T., Kukla, G.J., Heller, F., McCoy, W.D., Oches, E. A., Buggle, B., Zöller, L., 2011. The last million years recorded at the Stari Slankamen (North Serbia) loess-paleosol sequence: revised chronostratigraphy and long-term environmental trends. *Quat. Sci. Rev.* 30, 1142–1154. <https://doi.org/10.1016/j.quascirev.2011.02.004>.
- Marković, S.B., Stevens, T., Kukla, G.J., Hambach, U., Fitzsimmons, K.E., Gibbard, P.L., Buggle, B., Zech, M., Guo, Z., Hao, Q., Wu, H., O'Hara-Dhand, K., Smalley, I.J., Újvári, G., Sümeği, P., Timar-Gabor, A., Veres, D., Sirocko, F., Vasiljević, D.A., Jary, Z., Svensson, A.M., Jović, V., Lehmkuhl, F., Kovács, J.I., Svirčev, Z., 2015. Danube loess stratigraphy - Towards a pan-European loess stratigraphic model. *Earth-Sci. Rev.* 148, 228–258. <https://doi.org/10.1016/j.earscirev.2015.06.005>.
- Matenco, L., Andriessen, P.A.M., Avram, C., Bada, G., Beekman, F., Bielik, M., Ter Borgh, M., Cifici, G., Cvetković, V., Dinu, C., Dombardi, E., Dondurur, D., Ergun, M., Francu, J., Fügensschub, B., Garcia-Castellanos, D., Götz, J., Horváth, F., Houseman, G., Knežević, S., Kovac, M., Kralikova, S., Krijgsman, W., Kucuk, M., Legosteva, O., Lercolais, G., Jipa, D.C., Maximov, G., Melinte, M., Minar, J., Munteanu, I., Munt, I.J., Olariu, C., Otto, J.C., Panin, N., Plasienska, D., Reiser, M., Rundić, L., Rupprechter, M., Safanda, J., Schmid, S.M., Schrott, L., Schuster, R., Starostenko, V., Steel, R.J., Stephenson, R.A., Stovba, S., Sokoutis, D., Stankoviansky, M., Stoica, A.M., Stojadinović, U., Toljić, M., Tomljenović, B., Ter Voorde, M., Wong, H., 2013. Quantifying the mass transfer from mountain ranges to deposition in sedimentary basins: source to sink studies in the Danube basin-black

- sea system. *Glob. Planet. Chang.* 103, 1–18. <https://doi.org/10.1016/j.gloplacha.2013.01.003>.
- Meert, J.G., 2003. A synopsis of events related to the assembly of the eastern Gondwana. *Tectonophysics*. [https://doi.org/10.1016/S0040-1951\(02\)00629-7](https://doi.org/10.1016/S0040-1951(02)00629-7).
- Meert, J.G., 2012. What's in a name? The Columbia (Paleopangaea/Nuna) supercontinent. *Gondwana Res.* 21, 987–993. <https://doi.org/10.1016/j.gr.2011.12.002>.
- Meinhold, G., Kostopoulos, D., Frei, D., Himmerkus, F., Reischmann, T., 2010. U-Pb LA-SF-ICP-MS zircon geochronology of the Serbo-Macedonian Massif, Greece: Palaeotectonic constraints for Gondwana-derived terranes in the Eastern Mediterranean. *Int. J. Earth Sci.* 99, 813–832. <https://doi.org/10.1007/s00531-009-0425-5>.
- Meinhold, G., Morton, A.C., Avigad, D., 2013. New insights into peri-Gondwana paleogeography and the Gondwana super-fan system from detrital zircon U-Pb ages. *Gondwana Res.* 23, 661–665. <https://doi.org/10.1016/j.gr.2012.05.003>.
- Meira, V.T., García-Casco, A., Juliani, C., Almeida, R.P., Schorsch, J.H.D., 2015. The role of intracontinental deformation in supercontinent assembly: Insights from the Ribeira Belt, Southeastern Brazil (Neoproterozoic West Gondwana). *Terra Nova* 27, 206–217. <https://doi.org/10.1111/ter.12149>.
- Mentlik, P., Engel, Z., Braucher, R., Léanni, L., Arnold, M., Aumaître, G., Bourlés, D., Keddadouche, K., 2013. Chronology of the late Weichselian glaciation in the Bohemian Forest in Central Europe. *Quat. Sci. Rev.* 65, 120–128. <https://doi.org/10.1016/j.quascirev.2013.01.020>.
- Middleton, N.J., Betzer, P.R., Bull, P.A., 2001. Long-range transport of “giant” aeolian quartz grains: linkage with discrete sedimentary sources and implications for protective particle transfer. *Mar. Geol.* 177, 411–417.
- Muhs, D.R., 2013a. Loess and its Geomorphologic, Stratigraphic, and Paleoclimatic significance in the Quaternary. In: Shroder, J.F., Lancaster, N., Sherman, D.J., Baas, A.C.W. (Eds.), *Treatise on Geomorphology*. Academic Press, pp. 149–183. <https://doi.org/10.1016/B978-0-12-374739-6.00302-X>.
- Muhs, D.R., 2013b. The geologic records of dust in the Quaternary. *Aeolian Res.* 9, 3–48. <https://doi.org/10.1016/j.aeolia.2012.08.001>.
- Muhs, D.R., Bettis, E.A., 2003. Quaternary loess-paleosol sequences as examples of climate-driven sedimentary extremes. *Spec. Pap. Geol. Soc. Am.* 370, 53–74. <https://doi.org/10.1130/0-8137-2370-1.53>.
- Nance, R.D., Murphy, J.B., Strachan, R.A., Keppie, J.D., Gutiérrez-Alonso, G., Fernández-Suárez, J., Quesada, C., Linnemann, U., D'Lemos, R., Pisarevsky, S.A., 2008. Neoproterozoic-early Palaeozoic tectonostratigraphy and palaeogeography of the peri-Gondwanan terranes: Amazonian v. West African connections. In: Ennih, N., Liegeois, J.P. (Eds.), *The Boundaries of the West African Craton*. Geological Society, London, London, pp. 345–383.
- Nance, R.D., Gutiérrez-Alonso, G., Keppie, J.D., Linnemann, U., Murphy, J.B., Quesada, C., Strachan, R.A., Woodcock, N.H., 2010. Evolution of the Rheic Ocean. *Gondwana Res.* 17, 194–222. <https://doi.org/10.1016/j.gr.2009.08.001>.
- Nance, R.D., Gutiérrez-Alonso, G., Keppie, J.D., Linnemann, U., Murphy, J.B., Quesada, C., Strachan, R.A., Woodcock, N.H., 2012. A brief history of the Rheic Ocean. *Geosci. Front.* 3, 125–135. <https://doi.org/10.1016/j.gsf.2011.11.008>.
- Nemec, E., Pécsi, M., Hartyani, Z., Horváth, T., 2000. The origin of the silt size quartz grains and minerals in loess. *Quat. Int.* 68–71, 199–208.
- Nie, J., Stevens, T., Rittner, M., Stockli, D.F., Garzanti, E., Limonta, M., Vermeesch, P., Saylor, J.E., Lu, H., Breecker, D., Hu, X., Bird, A.F., Ando, S., Liu, S., Resentini, A., Vezzoli, G., Peng, W., Carter, A., Ji, S., Pan, B., 2015. Loess Plateau storage of Northeastern Tibetan Plateau-derived Yellow River sediment. *Nat. Commun.* 6. <https://doi.org/10.1038/ncomms9511>.
- Novothy, Á., Frechen, M., Horváth, E., Wacha, L., Rolf, C., 2011. Investigating the penultimate and last glacial cycles of the Süttő loess section (Hungary) using luminescence dating, high-resolution grain size, and magnetic susceptibility data. *Quat. Int.* 234, 75–85. <https://doi.org/10.1016/j.quaint.2010.08.002>.
- Nowell, G.M., Parrish, R.R., 2001. Simultaneous acquisition of isotope compositions and parent/daughter ratios by non-isotope dilution-mode plasma ionisation multi-collector mass spectrometry (PIMMS). In: Holland, G., Tanner, S.D. (Eds.), *Plasma Source Mass Spectrometry: The New Millennium*. Royal Society of Chemistry, Special Publications, pp. 298–310.
- Obrecht, I., Zeeden, C., Schulte, P., Hambach, U., Eckmeier, E., Timar-Gabor, A., Lehmkuhl, F., 2015. Aeolian dynamics at the Orlovat loess-paleosol sequence, northern Serbia, based on detailed textural and geochemical evidence. *Aeolian Res.* 18, 69–81. <https://doi.org/10.1016/j.aeolia.2015.06.004>.
- Obruchev, V.A., 1945. Loess types and their origin. *Am. J. Sci.* 243, 256–262.
- Oliver, G.J.H., Corfu, F., Krogh, T.E., 1993. U-Pb ages from SW Poland: evidence for a Caledonian suture zone between Baltica and Gondwana. *J. Geol. Soc.* 150, 355–369.
- Pańczyk, M., Nawrocki, J., Bogucki, A.B., Gozłik, P., Łanczont, M., 2020. Possible sources and transport pathways of loess deposited in Poland and Ukraine from detrital zircon U-Pb age spectra. *Aeolian Res.* 45. <https://doi.org/10.1016/j.aeolia.2020.100598>. A provenance study was carried out on loess deposit.
- Pastore, G., Baird, T., Vermeesch, P., Resentini, A., Garzanti, E., 2021. Provenance and recycling of Sahara Desert sand. *Earth-Sci. Rev.* 216, 103606. <https://doi.org/10.1016/j.earscirev.2021.103606>.
- Paton, C., Hellstrom, J., Paul, B., Woodhead, J.D., Hergt, J., 2011. Iolite: Freeware for the visualisation and processing of mass spectrometric data. *J. Anal. At. Spectrom.* 26, 2508–2518. <https://doi.org/10.1039/c1ja10172b>.
- Pavčić, D., Kovačić, M., Banak, A., Jiménez-Moreno, G., Marković, F., Pikelj, K., Vranjković, A., Premužak, L., Tibljaš, D., Belak, M., 2016. Early miocene European loess: a new record of aridity in southern Europe. *Bull. Geol. Soc. Am.* 128, 110–121. <https://doi.org/10.1130/B31280.1>.
- Pawlewicz, M.J., Steinsouer, D.W., Gautier, D.L., 2002. Map Showing Geology, Oil and Gas Fields, and Geologic Provinces of Europe including Turkey: Open-File Report 97-470-I. <https://doi.org/10.3133/ofr974701>.
- Peng, S., Hao, Q., Wang, L., Ding, M., Zhang, W., Wang, Y., Guo, Z., 2016. Geochemical and grain-size evidence for the provenance of loess deposits in the Central Shandong Mountains region, northern China. *Quat. Res. (United States)* 85, 290–298. <https://doi.org/10.1016/j.yqres.2016.01.005>.
- Persits, F.M., Ulmshiek, G.F., Steinsouer, D.W., 1999. Maps Showing Geology, Oil and Gas Fields and Geologic Provinces of the Former Soviet Union Open-File Report 97-470-E.
- Pfeifer, L.S., Soreghan, G.S., Pochat, S., Van Den Driessche, J., 2020. Loess in eastern equatorial Pangea archives a dusty atmosphere and possible upland glaciation. *Bull. Geol. Soc. Am.* 133, 379–392. <https://doi.org/10.1130/B35590.1>.
- Plissart, G., Diot, H., Monnier, C., MăruŃiu, M., Berger, J., 2012. Relationship between a syntectonic granitic intrusion and a shear zone in the Southern Carpathian-Balkan area (Almăj Mountains, Romania): implications for late Variscan kinematics and Cherbelezu granitoid emplacement. *J. Struct. Geol.* 39, 83–102. <https://doi.org/10.1016/j.jsg.2012.03.004>.
- Pöter, S., Veres, D., Baykal, Y., Nett, J.J., Schulte, P., Hambach, U., Lehmkuhl, F., 2021. Disentangling sedimentary pathways for the pleniglacial Lower Danube Loess based on geochemical signatures. *Front. Earth Sci.* 9, 1–25. <https://doi.org/10.3389/feart.2021.600010>.
- Pullen, A., Ibanez-Mejia, M., Gehrels, G.E., Ibanez-Mejia, J.C., Pecha, M., 2014. What happens when n = 1000? Creating large-n geochronological datasets with LA-ICP-MS for geologic investigations. *J. Anal. At. Spectrom.* 29, 971–980. <https://doi.org/10.1039/C4JA00024B>.
- Pye, K., 1995. The nature, origin and accumulation of loess. *Quat. Sci. Rev.* 14, 653–667. [https://doi.org/10.1016/0277-3791\(95\)00047-X](https://doi.org/10.1016/0277-3791(95)00047-X).
- Pye, K., Sperling, C.H.B., 1983. Experimental investigation of silt formation by static breakage processes: the effect of temperature, moisture and salt on quartz dune sand and granitic regolith. *Sedimentology* 30, 49–62. <https://doi.org/10.1111/j.1365-3091.1983.tb00649.x>.
- Rengers, F.K., Kean, J.W., Reitman, N.G., Smith, J.B., Coe, J.A., McGuire, L.A., 2020. The influence of frost weathering on debris flow sediment supply in an Alpine Basin. *J. Geophys. Res. Earth Surf.* 125. <https://doi.org/10.1029/2019JF005369>.
- Roberts, N.M.W., Slagstad, T., Parrish, R.R., Norry, M.J., Marker, M., Horstwood, M.S.A., 2013. Sedimentary recycling in arc magmas: geochemical and U-Pb-Hf-O constraints on the Mesoproterozoic Sudal Arc, SW Norway. *Contrib. Mineral. Petrol.* 165, 507–523. <https://doi.org/10.1007/s00410-012-0820-y>.
- Rosenbaum, G., Lister, G.S., 2005. The Western Alps from the Jurassic to Oligocene: spatio-temporal constraints and evolutionary reconstructions. *Earth-Sci. Rev.* 69, 281–306. <https://doi.org/10.1016/j.earscirev.2004.10.001>.
- Rousseau, D.-D., Antoine, P., Gerasimenko, N.P., Sima, A., Fuchs, M., Hatté, C., Moine, O., Zöller, L., 2011. North Atlantic abrupt climatic events of the last glacial period recorded in Ukrainian loess deposits. *Clim. Past* 7, 221–234. <https://doi.org/10.5194/cp-7-221-2011>.
- Ryder, C.L., Highwood, E.J., Lai, T.M., Sodemann, H., Marsham, J.H., 2013. Impact of atmospheric transport on the evolution of microphysical and optical properties of Saharan dust. *Geophys. Res. Lett.* 40, 2433–2438. <https://doi.org/10.1002/grl.50482>.
- Sarkkaya, M.A., Stepišnik, U., Žebre, M., Činer, A., Yıldırım, C., Vlahović, I., Tomljenović, B., Matoš, B., Wilcken, K.M., 2020. Last glacial maximum deglaciation of the Southern Velebit Mt. (Croatia): insights from cosmogenic ³⁶Cl dating of Rujanska Kosa. *Mediterr. Geosci. Rev.* 2, 53–64. <https://doi.org/10.1007/s42990-020-00030-9>.
- Savov, I., Ryan, J., Haydoutov, I., Schijf, J., 2001. Late Precambrian Balkan-Carpathian ophiolite — a slice of the Pan-African ocean crust?: geochemical and tectonic insights from the Tcherni Vrah and Deli Jovan massifs, Bulgaria and Serbia. *J. Volcanol. Geotherm. Res.* 110, 299–318. [https://doi.org/10.1016/S0377-0273\(01\)00216-5](https://doi.org/10.1016/S0377-0273(01)00216-5).
- Schaltegger, U., Abrecht, J., Corfu, F., 2003. The Ordovician orogeny in the Alpine basement: constraints from geochronology and geochemistry in the Aar Massif (Central Alps). *Swiss Bull. Mineral. Petrol.* 833, 183–195.
- Schatz, A.-K., Qi, Y., Siebel, W., Wu, J., Zöller, L., 2015. Tracking potential source areas of central European loess: examples from Tokaj (HU), Nussloch (D) and Grub (AT). *Open Geosci.* 7, 678–720. <https://doi.org/10.1515/geo-2015-0048>.
- Scherler, D., Bookhagen, B., Wulf, H., Preusser, F., Strecker, M.R., 2015. Increased late Pleistocene erosion rates during fluvial aggradation in the Garhwal Himalaya, northern India. *Earth Planet. Sci. Lett.* 428, 255–266. <https://doi.org/10.1016/j.epsl.2015.06.034>.
- Schmid, S.M., Bernoulli, D., Fügenschuh, B., Matenco, L., Schefer, S., Schuster, R., Tschirner, M., Ustaszewski, K., 2008. The Alpine-Carpathian-Dinaric orogenic system: correlation and evolution of tectonic units. *Swiss J. Geosci.* 101, 139–183. <https://doi.org/10.1007/s00015-008-1247-3>.
- Schmid, S.M., Fügenschuh, B., Kounov, A., Maţenco, L., Nievergelt, P., Oberhänsli, R., Pleuger, J., Schefer, S., Schuster, R., Tomljenović, B., Ustaszewski, K., van Hinsbergen, D.J.J., 2020. Tectonic units of the Alpine collision zone between Eastern Alps and western Turkey. *Gondwana Res.* 78, 308–374. <https://doi.org/10.1016/j.gr.2019.07.005>.
- Siegemund, S., Oriolo, S., Heinrichs, T., Basei, M.A.S., Nolte, N., Hüttenrauch, F., Schulz, B., 2018. Provenance of Austroalpine basement metasediments: tightening up Early Palaeozoic connections between peri-Gondwanan domains of central Europe and Northern Africa. *Int. J. Earth Sci.* 107, 2293–2315. <https://doi.org/10.1007/s00531-018-1599-5>.
- Skonieczny, C., Bory, A., Bout-Roumazilles, V., Abouchami, W., Galer, S.J.G., Crosta, X., Diallo, A., Ndiaye, T., 2013. A three-year time series of mineral dust deposits on the

- West African margin: Sedimentological and geochemical signatures and implications for interpretation of marine paleo-dust records. *Earth Planet. Sci. Lett.* 364, 145–156. <https://doi.org/10.1016/j.epsl.2012.12.039>.
- Skurzyski, J., Jary, Z., Kenis, P., Kubik, R., Moska, P., Raczky, J., Seul, C., 2020. Geochemistry and mineralogy of the late Pleistocene loess-paleosol sequence in Złota (near Sandomierz, Poland): implications for weathering, sedimentary recycling and provenance. *Geoderma* 375. <https://doi.org/10.1016/j.geoderma.2020.114459>.
- Sláma, J., Košler, J., Condon, D.J., Crowley, J.L., Gerdes, A., Hanchar, J.M., Horstwood, M.S.A., Morris, G.A., Nasdala, L., Norberg, N., Schaltegger, U., Schoene, B., Tubrett, M.N., Whitehouse, M.J., 2008. Plešovice zircon — a new natural reference material for U–Pb and Hf isotopic microanalysis. *Chem. Geol.* 249, 1–35. <https://doi.org/10.1016/j.chemgeo.2007.11.005>.
- Smalley, I.J., 1966. The properties of glacial loess and the formation of loess deposits. *J. Sediment. Res.* 36, 669–676. <https://doi.org/10.1306/74d7153c-2b21-11d7-8648000102c1865d>.
- Smalley, I.J., 2008. A call for Australian loess: discussion and commentary. *Area* 40, 131–134. <https://doi.org/10.1111/j.1475-4762.2008.00795.x>.
- Smalley, I.J., Derbyshire, E., 1990. The definition of “ice-sheet” and “mountain” loess. *Area* 22, 300–301.
- Smalley, I.J., Leach, J.A., 1978. The origin and distribution of the loess in the Danube basin and associated regions of East-Central Europe — a review. *Sediment. Geol.* 21, 1–26. [https://doi.org/10.1016/0037-0738\(78\)90031-3](https://doi.org/10.1016/0037-0738(78)90031-3).
- Smalley, I.J., Vita-Finzi, C., 1968. The formation of fine particles in Sandy deserts and the nature of “desert” loess. *J. Sediment. Petrol.* 38, 766–774. <https://doi.org/10.1306/74d71a69-2b21-11d7-8648000102c1865d>.
- Smalley, I.J., O'Hara-Dhand, K., Wint, J., Machalet, B., Jary, Z., Jefferson, I.F., 2009. Rivers and loess: the significance of long river transportation in the complex event-sequence approach to loess deposit formation. *Quat. Int.* 198, 7–18. <https://doi.org/10.1016/j.quaint.2008.06.009>.
- Smalley, I.J., Marshall, J., Fitzsimmons, K.E., Whalley, W.B., Ngambi, S., 2019. Desert loess: a selection of relevant topics. *Geologos* 25, 91–102. <https://doi.org/10.2478/logos-2019-0007>.
- Smith, B.J., Wright, J.S., Whalley, W.B., 1991. Simulated aeolian abrasion of Pannonian Sands and its implications for the origins of Hungarian Loess. *Earth Surf. Process. Landf.* 16, 745–752.
- Smith, B.J., Wright, J.S., Whalley, W.B., 2002. Sources of non-glacial, loess-size quartz silt and the origins of “desert loess”. *Earth-Sci. Rev.* 59, 1–26. [https://doi.org/10.1016/S0012-8252\(02\)00066-1](https://doi.org/10.1016/S0012-8252(02)00066-1).
- Söderlund, U., Patchett, P.J., Vervoort, J.D., Isachsen, C.E., 2004. The ¹⁷⁶Lu decay constant determined by Lu–Hf and U–Pb isotope systematics of Precambrian mafic intrusions. *Earth Planet. Sci. Lett.* 219, 311–324. [https://doi.org/10.1016/S0012-821X\(04\)00012-3](https://doi.org/10.1016/S0012-821X(04)00012-3).
- Soreghan, G.S., Soreghan, M.J., Hamilton, M.A., 2008. Origin and significance of loess in late Palaeozoic western Pangaea: a record of tropical cold? *Palaeogeogr. Palaeoclimatol. Palaeoecol.* 268, 234–259. <https://doi.org/10.1016/j.palaeo.2008.03.050>.
- Soreghan, G.S., Joo, Y.J., Elwood Madden, M.E., Van Deventer, S.C., 2016. Silt production as a function of climate and lithology under simulated comminution. *Quat. Int.* 399, 218–227. <https://doi.org/10.1016/j.quaint.2015.05.010>.
- Spencer, C.J., Hawkesworth, C.J., Cawood, P.A., Dhuime, B., 2013. Not all supercontinents are created equal: Gondwana–Rodinia case study. *Geology* 41, 795–798. <https://doi.org/10.1130/G34520.1>.
- Squire, R.J., Campbell, I.H., Allen, C.M., Wilson, C.J.L., 2006. Did the Transgondwanan Supermountain trigger the explosive radiation of animals on Earth? *Earth Planet. Sci. Lett.* 250, 116–133. <https://doi.org/10.1016/j.epsl.2006.07.032>.
- Stampfli, G.M., Borel, G.D., 2002. A plate tectonic model for the Paleozoic and Mesozoic constrained by dynamic plate boundaries and restored synthetic oceanic isochrons. *Earth Planet. Sci. Lett.* 196, 17–33. [https://doi.org/10.1016/S0012-821X\(01\)00588-X](https://doi.org/10.1016/S0012-821X(01)00588-X).
- Stampfli, G.M., Von Raumer, J.F., Borel, G.D., 2002. Paleozoic evolution of pre-Variscan terranes: from Gondwana to the Variscan collision. *Spec. Pap. Geol. Soc. Am.* 364, 263–280. <https://doi.org/10.1130/0-8137-2364-7.263>.
- Stampfli, G.M., Hochard, C., Vêrard, C., Wilhelm, C., VonRaumer, J., 2013. The formation of Pangea. *Tectonophysics* 593, 1–19. <https://doi.org/10.1016/j.tecto.2013.02.037>.
- Stephan, T., Kroner, U., Romer, R.L., Rösel, D., 2019. From a bipartite Gondwanan shelf to an arcuate Variscan belt: the early Paleozoic evolution of northern Peri-Gondwana. *Earth-Sci. Rev.* 192, 491–512. <https://doi.org/10.1016/j.earscirev.2019.03.012>.
- Stern, R.J., 1994. Arc assembly and continental collision in the Neoproterozoic East African Orogen: Implications for the consolidation of Gondwanaland. *Annu. Rev. Anthropol.* 22, 319–351.
- Stevens, T., Palk, C., Carter, A., Lu, H., Clift, P.D., 2010. Assessing the provenance of loess and desert sediments in northern China using U–Pb dating and morphology of detrital zircons. *Geol. Soc. Am. Bull.* 122, 1331–1344. <https://doi.org/10.1130/B30102.1>.
- Stevens, T., Carter, A., Watson, T.P., Vermeesch, P., Andò, S., Bird, A.F., Lu, H., Garzanti, E., Cottam, M.A., Sevastjanova, I., 2013. Genetic linkage between the Yellow River, the Mu Us desert and the Chinese Loess Plateau. *Quat. Sci. Rev.* 78, 355–368. <https://doi.org/10.1016/j.quascirev.2012.11.032>.
- Strömsoe, J.R., Paasche, Ø., 2011. Weathering patterns in high-latitude regolith. *J. Geophys. Res. Earth Surf.* 116. <https://doi.org/10.1029/2010JF001954>.
- Stuut, J.B., Smalley, I.J., O'Hara-Dhand, K., 2009. Aeolian dust in Europe: African sources and European deposits. *Quat. Int.* 198, 234–245. <https://doi.org/10.1016/j.quaint.2008.10.007>.
- Sun, J., 2002. Provenance of loess material and formation of loess deposits on the Chinese Loess Plateau. *Earth Planet. Sci. Lett.* 203, 845–859. [https://doi.org/10.1016/S0012-821X\(02\)00921-4](https://doi.org/10.1016/S0012-821X(02)00921-4).
- Thamó-Bozó, E., Kovács, L.O., Magyari, Á., Marsi, I., 2014. Tracing the origin of loess in Hungary with the help of heavy mineral composition data. *Quat. Int.* 319, 11–21. <https://doi.org/10.1016/j.quaint.2013.04.030>.
- Torsvik, T.H., Rehnström, E.F., 2003. The Tornquist Sea and Baltica–Avalonia docking. *Tectonophysics* 362, 67–82. [https://doi.org/10.1016/S0040-1951\(02\)00631-5](https://doi.org/10.1016/S0040-1951(02)00631-5).
- Trench, A., Torsvik, T.H., 1992. The closure of the Iapetus Ocean and Tornquist Sea: new palaeomagnetic constraints. *J. Geol. Soc.* 149, 867–870. <https://doi.org/10.1144/gsjgs.149.6.0867>.
- Tsoar, H., Pye, K., 1987. Dust transport and the question of desert loess formation. *Sedimentology* 34, 139–153. <https://doi.org/10.1111/j.1365-3091.1987.tb00566.x>.
- Újvári, G., Klötzli, U., 2015. U–Pb ages and Hf isotopic composition of zircons in Austrian last glacial loess: constraints on heavy mineral sources and sediment transport pathways. *Int. J. Earth Sci.* 104, 1365–1385. <https://doi.org/10.1007/s00531-014-1139-x>.
- Újvári, G., Varga, A., Balogh-Brunstad, Z., 2008. Origin, weathering, and geochemical composition of loess in southwestern Hungary. *Quat. Res.* 69, 421–437. <https://doi.org/10.1016/j.yqres.2008.02.001>.
- Újvári, G., Ramos, F.C., Dimond, C., Kovács, J.I., Varga, G., Varga, A., 2010. On possible sources of loess deposits in the Carpathian Basin: an isotopic approach. *Geophys. Res. Abstr.* 9–10.
- Újvári, G., Varga, A., Ramos, F.C., Kovács, J.I., Németh, T., Stevens, T., 2012. Evaluating the use of clay mineralogy, Sr–Nd isotopes and zircon U–Pb ages in tracking dust provenance: an example from loess of the Carpathian Basin. *Chem. Geol.* 304–305, 83–96. <https://doi.org/10.1016/j.chemgeo.2012.02.007>.
- Újvári, G., Klötzli, U., Kiraly, F., Ntafos, T., 2013. Towards identifying the origin of metamorphic components in Austrian loess: insights from detrital rutile chemistry, thermometry and U–Pb geochronology. *Quat. Sci. Rev.* 75, 132–142. <https://doi.org/10.1016/j.quascirev.2013.06.002>.
- Újvári, G., Varga, A., Raucsik, B., Kovács, J.I., 2014. The Paks loess-paleosol sequence: a record of chemical weathering and provenance for the last 800ka in the mid-Carpathian Basin. *Quat. Int.* 319, 22–37. <https://doi.org/10.1016/j.quaint.2012.04.004>.
- Újvári, G., Kok, J.F., Varga, G., Kovács, J.I., 2016. The physics of wind-blown loess: implications for grain size proxy interpretations in Quaternary paleoclimate studies. *Earth-Sci. Rev.* 154, 247–278. <https://doi.org/10.1016/j.earscirev.2016.01.006>.
- Urdea, P., Onaca, A., Ardelean, F., Ardelean, M., 2011. New evidence on the quaternary glaciation in the Romanian carpathians. *Dev. Quat. Sci.* 2, 305–322. <https://doi.org/10.1016/B978-0-444-53447-7.00024-6>.
- Van Der Does, M., Korte, L.F., Munday, C.I., Brummer, G.-J.A., Stuut, J.-B.W., 2016. Particle size traces modern Saharan dust transport and deposition across the equatorial North Atlantic. *Atmos. Chem. Phys.* 16, 13697–13710. <https://doi.org/10.5194/acp-16-13697-2016>.
- Van Der Does, M., Knippertz, P., Zschenderlein, P., Harrison, R.G., Stuut, J.-B.W., 2018. The mysterious long-range transport of giant mineral dust particles. *Sci. Adv.* 4, 1–9.
- van Hinsbergen, D.J.J., Torsvik, T.H., Schmid, S.M., Matenco, L.C., Maffione, M., Vissers, R.L.M., Gürrer, D., Spakman, W., 2020. Orogenic architecture of the Mediterranean region and kinematic reconstruction of its tectonic evolution since the triassic. *Gondwana Res.* 81, 79–229. <https://doi.org/10.1016/j.gr.2019.07.009>.
- Vandenbergh, J., Marković, S.B., Jovanović, M., Hambach, U., 2014. Site-specific variability of loess and paleosols (Ruma, Vojvodina, northern Serbia). *Quat. Int.* 334–335, 86–93. <https://doi.org/10.1016/j.quaint.2013.10.036>.
- Varga, A., Újvári, G., Raucsik, B., 2011. Tectonic versus climatic control on the evolution of a loess-paleosol sequence at Beremend, Hungary: an integrated approach based on paleoecological, clay mineralogical, and geochemical data. *Quat. Int.* 240, 71–86. <https://doi.org/10.1016/j.quaint.2010.10.032>.
- Varga, G., Kovács, J.I., Újvári, G., 2013. Analysis of Saharan dust intrusions into the Carpathian Basin (Central Europe) over the period of 1979–2011. *Glob. Planet. Chang.* 100, 333–342. <https://doi.org/10.1016/j.gloplacha.2012.11.007>.
- Varga, G., Cserhádi, C., Kovács, J.I., Szalai, Z., 2016. Saharan dust deposition in the Carpathian Basin and its possible effects on interglacial soil formation. *Aeolian Res.* 22, 1–12. <https://doi.org/10.1016/j.aeolia.2016.05.004>.
- Varga, G., Újvári, G., Kovács, J.I., 2019. Interpretation of sedimentary (sub)populations extracted from grain size distributions of central European loess-paleosol series. *Quat. Int.* 502, 60–70. <https://doi.org/10.1016/j.quaint.2017.09.021>.
- Varga, G., Dagsson-Walhausserová, P., Gresina, F., Helgadottir, A., 2021. Saharan dust and giant quartz particle transport towards Iceland. *Sci. Rep.* 11, 1–12. <https://doi.org/10.1038/s41598-021-91481-z>.
- Veivers, J.J., 2003. Pan-African is Pan-Gondwanaland: oblique convergence drives rotation during 650–500 Ma assembly. *Geology* 31, 501–504. [https://doi.org/10.1130/0091-7613\(2003\)031<0501:PIPOCD>2.0.CO;2](https://doi.org/10.1130/0091-7613(2003)031<0501:PIPOCD>2.0.CO;2).
- Veivers, J.J., 2007. Pan-Gondwanaland post-collisional extension marked by 650–500 Ma alkaline rocks and carbonatites and related detrital zircons: a review. *Earth-Sci. Rev.* 83, 1–47. <https://doi.org/10.1016/j.earscirev.2007.03.001>.
- Vermeesch, P., 2004. How many grains are needed for a provenance study? *Earth Planet. Sci. Lett.* 224, 441–451. <https://doi.org/10.1016/j.epsl.2004.05.037>.
- Vermeesch, P., 2012. On the visualisation of detrital age distributions. *Chem. Geol.* 312–313, 190–194. <https://doi.org/10.1016/j.chemgeo.2012.04.021>.
- Vermeesch, P., 2013. Multi-sample comparison of detrital age distributions. *Chem. Geol.* 341, 140–146. <https://doi.org/10.1016/j.chemgeo.2013.01.010>.
- Vermeesch, P., 2018a. IsoplotR: a free and open toolbox for geochronology. *Geosci. Front.* 9, 1479–1493. <https://doi.org/10.1016/j.gsf.2018.04.001>.
- Vermeesch, P., 2018b. Dissimilarity measures in detrital geochronology. *Earth-Sci. Rev.* 178, 310–321. <https://doi.org/10.1016/j.earscirev.2017.11.027>.

- Vermeesch, P., Garzanti, E., 2015. Making geological sense of 'Big Data' in sedimentary provenance analysis. *Chem. Geol.* 409, 20–27. <https://doi.org/10.1016/j.chemgeo.2015.05.004>.
- von Raumer, J.F., Stampfli, G.M., Bussy, F., 2003. Gondwana-derived microcontinents - the constituents of the Variscan and Alpine collisional orogens. *Tectonophysics* 365, 7–22. [https://doi.org/10.1016/S0040-1951\(03\)00015-5](https://doi.org/10.1016/S0040-1951(03)00015-5).
- von Raumer, J.F., Bussy, F., Schaltegger, U., Schulz, B., Stampfli, G.M., 2013. Pre-mesozoic alpine basements-their place in the European paleozoic framework. *Bull. Geol. Soc. Am.* 125, 89–108. <https://doi.org/10.1130/B30654.1>.
- von Raumer, J.F., Stampfli, G.M., Arenas, R., Sánchez Martínez, S., 2015. Ediacaran to Cambrian oceanic rocks of the Gondwana margin and their tectonic interpretation. *Int. J. Earth Sci.* 104, 1107–1121. <https://doi.org/10.1007/s00531-015-1142-x>.
- Walczak, A., Belka, Z., 2017. Fingerprinting Gondwana versus Baltica provenance: Nd and Sr isotopes in Lower Paleozoic clastic rocks of the Malopolska and Łysogóry terranes, southern Poland. *Gondwana Res.* 45, 138–151. <https://doi.org/10.1016/j.gr.2017.02.002>.
- Wang, W., Cawood, P.A., Pandit, M.K., Zhao, J.H., Zheng, J.P., 2019. No collision between Eastern and Western Gondwana at their northern extent. *Geology* 47, 308–312. <https://doi.org/10.1130/G45745.1>.
- Wiedenbeck, M., Allé, P., Corfu, F., Griffin, W.L., Meier, M., Oberli, F., von Quadt, A., Roddick, J.C., Spiegel, W., 1995. Three natural zircon standards for U-Th-Pb, Lu-Hf, element and REE analyses. *Geostand. Newslett.* 19, 1–23. <https://doi.org/10.1111/j.1751-908X.1995.tb00147.x>.
- Wolf, D., Ryborz, K., Kolb, T., Calvo Zapata, R., Sanchez Vizcaino, J., Zöller, L., Faust, D., 2019. Origins and genesis of loess deposits in central Spain, as indicated by heavy mineral compositions and grain-size variability. *Sedimentology* 66, 1139–1161. <https://doi.org/10.1111/sed.12539>.
- Woodhead, J.D., Hergt, J.M., 2005. A preliminary appraisal of seven natural zircon reference materials for in situ Hf isotope determination. *Geostand. Geoanal. Res.* 29, 183–195. <https://doi.org/10.1111/j.1751-908X.2005.tb00891.x>.
- Wright, J.S., 1995. Glacial comminution of quartz sand grains and the production of loessic silt: a simulation study. *Quat. Sci. Rev.* 14, 669–680. [https://doi.org/10.1016/0277-3791\(95\)00048-8](https://doi.org/10.1016/0277-3791(95)00048-8).
- Wright, J.S., 2001. "Desert" loess versus "glacial" loess: quartz silt formation, source areas and sediment pathways in the formation of loess deposits. *Geomorphology* 36, 231–256. [https://doi.org/10.1016/S0169-555X\(00\)00060-X](https://doi.org/10.1016/S0169-555X(00)00060-X).
- Wright, J.S., 2007. An overview of the role of weathering in the production of quartz silt. *Sediment. Geol.* 202, 337–351. <https://doi.org/10.1016/j.sedgeo.2007.03.024>.
- Wright, J.S., Smith, B.J., 1993. Fluvial comminution and the production of loess-sized Quartz Silt: a simulation study. *Geogr. Ann. Ser. A. Phys. Geogr.* 75, 25–34.
- Wright, J.S., Smith, B.J., Whalley, B., 1998. Mechanisms of loess-sized quartz silt production and their relative effectiveness: Laboratory simulations. *Geomorphology* 23, 15–34. [https://doi.org/10.1016/S0169-555X\(97\)00084-6](https://doi.org/10.1016/S0169-555X(97)00084-6).
- Xia, D., Wang, Y., Jia, J., Wei, H., Fan, Y., Jin, M., Chen, F., 2020. Mountain loess or desert loess? New insight of the sources of Asian atmospheric dust based on mineral magnetic characterization of surface sediments in NW China. *Atmos. Environ.* 232, 117564. <https://doi.org/10.1016/j.atmosenv.2020.117564>.
- Zan, J., Li, X., Kang, J., Guo, Z., Mao, Z., 2020. Intensified pedogenesis caused the increase in the fine particle content of late Cenozoic fluvial and lacustrine deposits in the NE Tibetan Plateau. *Sediment. Geol.* 398, 105587. <https://doi.org/10.1016/j.sedgeo.2019.105587>.
- Zeh, A., Gerdes, A., 2010. Baltica- and Gondwana-derived sediments in the Mid-German Crystalline rise (Central Europe): Implications for the closure of the Rheic Ocean. *Gondwana Res.* 17, 254–263. <https://doi.org/10.1016/j.gr.2009.08.004>.
- Zhang, P., Najman, Y., Mei, L., Millar, I.L., Sobel, E.R., Carter, A., Barfod, D., Dhuime, B., Garzanti, E., Govin, G., Vezzoli, G., Hu, X., 2019. Palaeodrainage evolution of the large rivers of East Asia, and Himalayan-Tibet tectonics. *Earth-Sci. Rev.* 192, 601–630. <https://doi.org/10.1016/j.earscirev.2019.02.003>.
- Zhang, Haobo, Nie, J., Liu, X., Pullen, A., Li, G., Peng, W., Zhang, Hanzhi, 2021. Spatially variable provenance of the Chinese Loess Plateau. *Geology* XX, 1–5. <https://doi.org/10.1130/g48867.1>.
- Zlatkin, O., Avigad, D., Gerdes, A., 2018. New detrital zircon geochronology from the cycladic basement (Greece): implications for the Paleozoic Accretion of Peri-Gondwanan Terranes to Laurussia. *Tectonics* 37, 4679–4699. <https://doi.org/10.1029/2018TC005046>.
- Zurbruggen, R., 2015. Ordovician orogeny in the Alps: a reappraisal. *Int. J. Earth Sci.* 104, 335–350. <https://doi.org/10.1007/s00531-014-1090-x>.
- Zurbruggen, R., 2017. The Cenerian orogeny (early Paleozoic) from the perspective of the Alpine region. *Int. J. Earth Sci.* 106, 517–529. <https://doi.org/10.1007/s00531-016-1438-5>.